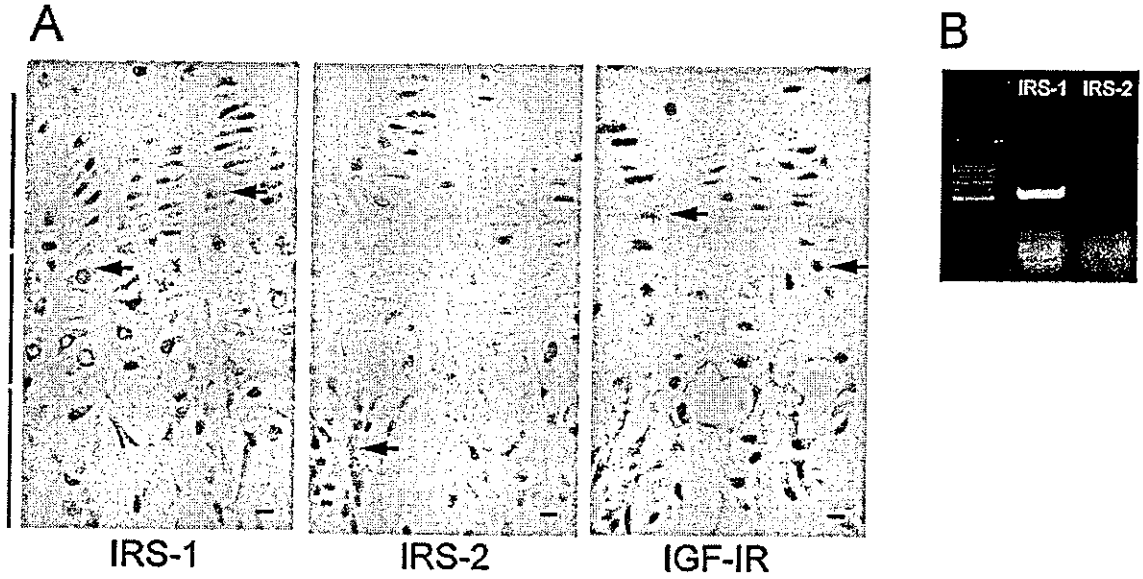

FIG. 1. (A) Immunolocalizations of IRS-1, IRS-2, and IGF-I receptor (IGF-IR) and (B) mRNA expressions of IRS-1 and IRS-2 in and around the epiphyseal cartilage of the proximal tibias of 5-week-old WT mice. (A) Blue, red, and green bars indicate layers of proliferative zone, hypertrophic zone, and primary spongiosa, respectively. Immunolocalization of IRS-1, shown in brown, was evident in chondrocytes of various differentiation stages (arrows) and osteoblasts in the primary spongiosa, although that of IRS-2 was not seen in chondrocytes, but in the bone cells including osteoclastic cells (arrow). Localization of IGF-IR was widely observed in chondrocytes (arrows), osteoblasts, and endothelial cells of blood vessels. No immunostaining was observed by the control non-immune IgG and IgY (data not shown). Bar, 10 μm. (B) Expression of IRS-1 and IRS-2 in the tibial epiphyseal cartilage isolated from WT mice determined by RT-PCR. IRS-2 expression was not seen even when the amount of template cDNA or the number of amplification cycles was increased.

Morphological findings of the proliferative zone of the IRS-1$^{-/-}$ cartilage

We compared the proliferative zone of the epiphyseal cartilage at 12 weeks between IRS-1$^{-/-}$ and WT mice (Fig. 3). PCNA^{+} cells that are known to have proliferative ability were seen in the WT proliferative zone; however, few were found in the IRS-1$^{-/-}$ cartilage. The PTH/PTHrP receptor (PPR) immunolocalization, a marker of the proliferative and prehypertrophic chondrocytes, was also decreased in the IRS-1$^{-/-}$ cartilage.

Morphological findings of the hypertrophic zone of the IRS-1$^{-/-}$ cartilage

We further compared the hypertrophic zone of the epiphyseal cartilage (Fig. 4). Type X collagen, a marker for hypertrophic chondrocytes, was similarly immunolocalized in the lower layer of the epiphyseal cartilage of both WT and IRS-1$^{-/-}$ mice at 3 weeks (Fig. 4A). At 12 weeks, it remained immunolocalized at the hypertrophic zone in WT mice, although the size of hypertrophic chondrocytes became smaller (Fig. 4B, top). In the IRS-1$^{-/-}$ cartilage, however, the staining became fainter but more extensive, localizing in even smaller hypertrophic chondrocytes than WT (Fig. 4B, top). TUNEL-staining revealed that these small hypertrophic chondrocytes included a considerable number of apoptotic cells that were rarely seen in the WT cartilage at this age (Fig. 4B, middle). Because TUNEL^{+} cells were hardly seen in the proliferative zone as previously reported,[33] the decrease in its height seems mainly caused by the reduction of proliferative ability of chondrocytes but not because of the accelerated apoptosis in this layer. In addition, the calcified matrix positively stained with von Kossa was surrounding the chondrocytes in all directions, and it covered the bottom of the hypertrophic zone in IRS-1$^{-/-}$ cartilage, although it was intermittently seen in the WT cartilage (Fig. 4B, bottom). In the ultrastructural finding of the bottom of the hypertrophic zone of the WT cartilage, the lacunae of hypertrophic chondrocytes were open to the marrow cavity with the invasion of blood vessels and osteoclasts (Fig. 4C). In the IRS-1$^{-/-}$ cartilage, however, much smaller chondrocytes were surrounded by the calcified matrix so that cartilage lacunae were not open to the marrow cavity, indicating that the epiphyseal cartilage had already been closed at 12 weeks.

Morphological findings of the primary spongiosa of the IRS-1$^{-/-}$ mice

At 12 weeks, the volume of primary spongiosa beneath the epiphyseal cartilage was much smaller in IRS-1$^{-/-}$ mice

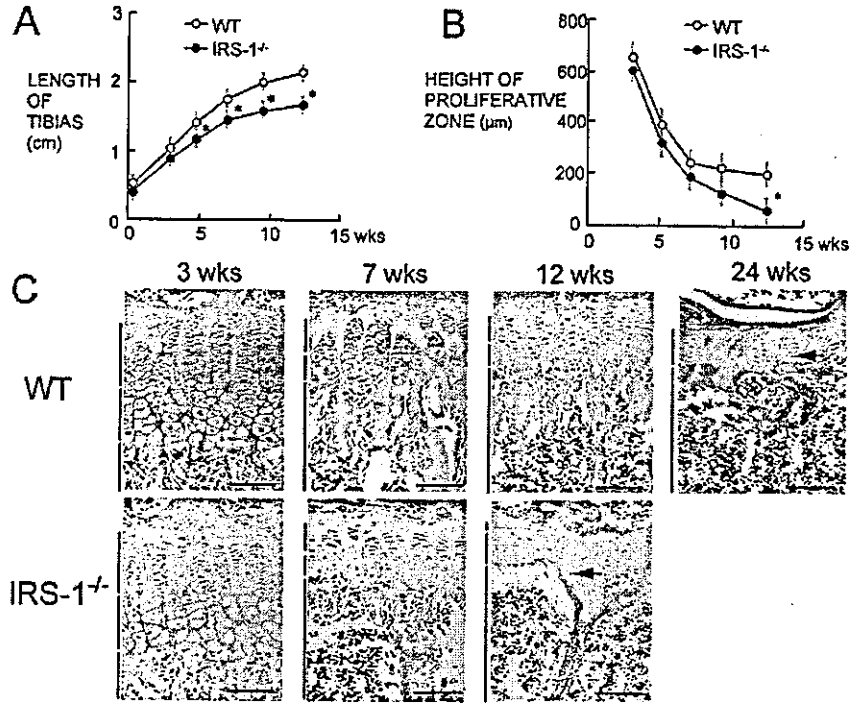

FIG. 2. Chronological changes in and around the tibial epiphyseal cartilage of WT and IRS-$1^{-/-}$ mice. (A) Time course of the length of WT and IRS-$1^{-/-}$ tibias. Data are expressed as means (symbols) ± SD (error bars) for 12 bones/group for WT and IRS-$1^{-/-}$. *$p < 0.01$ vs. WT. (B) Time course of the height of the proliferative zone in the WT and IRS-$1^{-/-}$ epiphyseal cartilage. Data are expressed as means (symbols) ± SD (error bars) for 6–12 bones/group for WT and IRS-$1^{-/-}$. *$p < 0.01$ vs. WT. (C) Time course of histological findings (HE staining) in and around the WT (top) and IRS-$1^{-/-}$ (bottom) epiphyseal cartilage. The chronological changes were accelerated in the IRS-$1^{-/-}$ cartilage compared with WT. In the IRS-$1^{-/-}$ cartilage at 12 weeks, the proliferative zone was hardly visible, and the size of hypertrophic chondrocytes was decreased (arrows), which resembled the findings of the WT cartilage at 24 weeks. Blue, red, and green bars indicate layers of proliferative zone, hypertrophic zone, and primary spongiosa, respectively. Bar, 100 μm.

than in WT mice. ALP^+ areas indicating active osteoblasts were accordingly decreased in IRS-$1^{-/-}$ mice (Fig. 5A). At the TEM level, spindle-shaped osteoblasts producing unmineralized osteoid entirely covered the bone surface in WT, whereas in IRS-$1^{-/-}$ mice, osteoblasts with a more flattened shape were intermittently seen on the mineralized bone without the osteoid intervention. To examine the bone turnover we performed the double staining of TRACP and osteopontin (Fig. 5B). $TRACP^+$ osteoclasts were also decreased in number in the IRS-$1^{-/-}$ spongiosa compared with WT. Osteopontin is known to be localized at the calcification front and the cement line.[34,35] It was diffusely localized in the bottom of the IRS-$1^{-/-}$ hypertrophic zone, which von Kossa staining confirmed was covered by the calcified matrix. In the IRS-$1^{-/-}$ bone collar, however, osteopontin-positive cement lines, indicating the sites of ongoing bone remodeling, were greatly decreased.

Histomorphometrical measurements supported these findings. In IRS-$1^{-/-}$ mice, bone volume was decreased to one-half that of WT mice, and parameters for both bone formation and resorption were significantly lower than those of WT, indicating osteopenia of a low-turnover state (Fig. 6A). The immunohistochemical finding showing the decrease in the number of $PCNA^+$ osteoblastic cells in the IRS-$1^{-/-}$ bone suggests the contribution of the suppression of osteoblast proliferation to the decreased bone turnover (Fig. 6B).

DISCUSSION

This study morphologically investigated the cellular mechanism by which IRS-1 deficiency causes skeletal growth retardation. The IRS-$1^{-/-}$ epiphyseal cartilage exhibited insufficient proliferation of chondrocytes, calcification of hypertrophic chondrocytes, acceleration of apoptosis, and early closure of the growth plate. It is therefore postulated that the IRS-1 signaling prevents the closure of this cartilage at an early age.

IRS-1 and IRS-2 signalings are reported to have distinct biological roles and to be differentially expressed in a variety of cells. Regarding glucose homeostasis, IRS-1 plays an important role in the metabolic actions of insulin and IGF-I mainly in skeletal muscle and adipose tissue, whereas IRS-2 does so in the liver.[36,37] We have reported

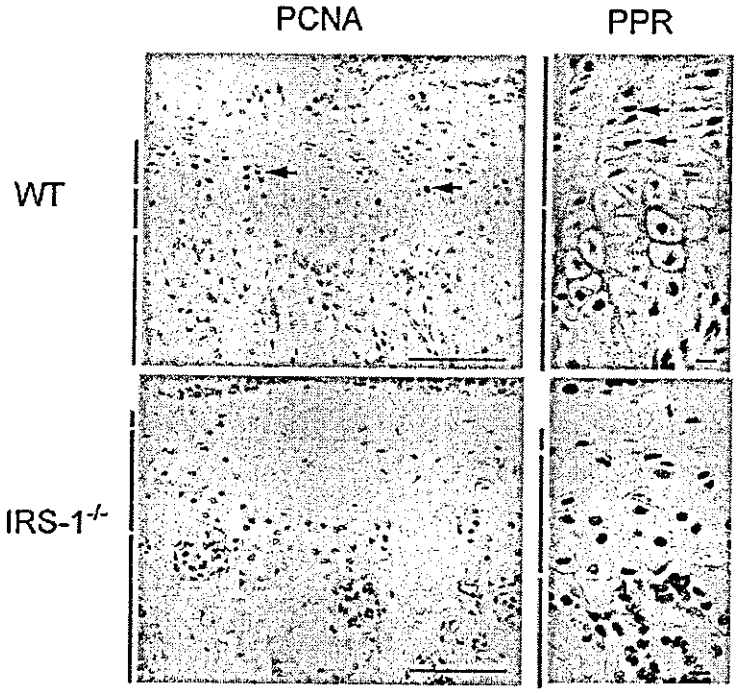

FIG. 3. Immunolocalizations of PCNA and PPR in the tibial epiphyseal cartilage of 12-week-old WT and IRS-$1^{-/-}$ mice. Both $PCNA^+$ cells (left, arrows) and PPR^+ cells (right, arrows) observed in the proliferative chondrocytes of WT mice (top) were hardly seen in the IRS-$1^{-/-}$ cartilage (bottom). Blue, red, and green bars indicate layers of proliferative zone, hypertrophic zone, and primary spongiosa, respectively. No immunostaining was observed by the control non-immune IgG (data not shown). Bar of the left panel, 100 μm. Bar of right panel, 10 μm.

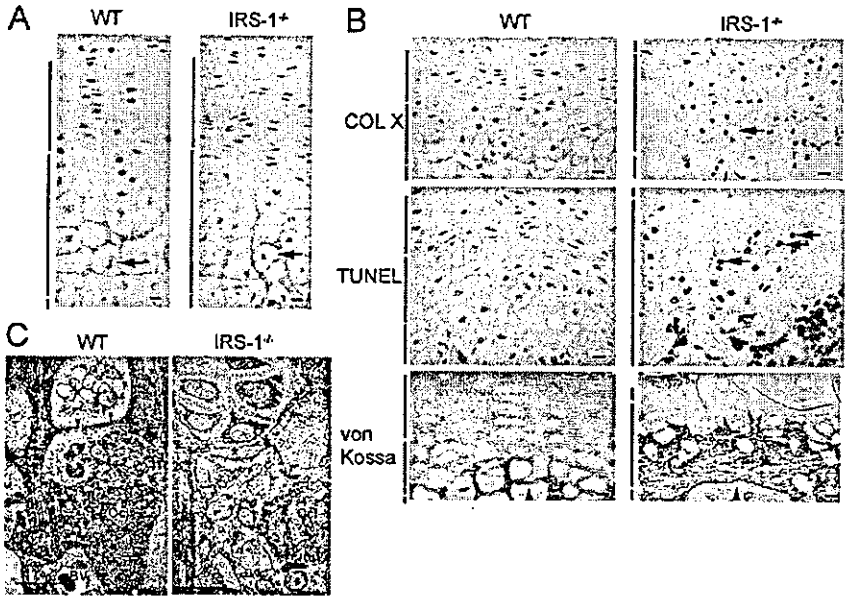

FIG. 4. Histochemical and ultrastructural findings in the hypertrophic zone of the WT and IRS-$1^{-/-}$ epiphyseal cartilage. (A) Immunostaining of type X collagen at 3 weeks. Localization of type X collagen-positive hypertrophic chondrocytes indicated by arrows was similar at 3 weeks. (B) Immunostainings of type X collagen (top), TUNEL (middle), and von Kossa (bottom) at 12 weeks. Type X collagen immunolocalization and size of hypertrophic chondrocytes (arrow, top) were different between WT and IRS-$1^{-/-}$ at this age. $TUNEL^+$ apoptotic cells were rarely seen in the WT cartilage, but they were distributed broadly in the IRS-$1^{-/-}$ hypertrophic chondrocytes (arrows, middle). No immunostaining was observed by the control non-immune IgG (data not shown). von Kossa–positive calcified matrix was seen intermittently in WT and continuously in IRS-$1^{-/-}$. Arrowheads indicate the site of vascular invasion. (C) Ultrastructural findings of the bottom of the hypertrophic zone by TEM at 12 weeks. Lacunae of hypertrophic chondrocytes were open to the marrow cavity in WT mice (arrowheads), although the IRS-$1^{-/-}$ chondrocytes were separated from the marrow by the calcified tissue (asterisks), indicating closure of the epiphyseal cartilage. BV, blood vessel; Ocl, osteoclasts. Blue, red, and green bars in A and B indicate layers of proliferative zone, hypertrophic zone, and primary spongiosa, respectively. Bar, 10 μm.

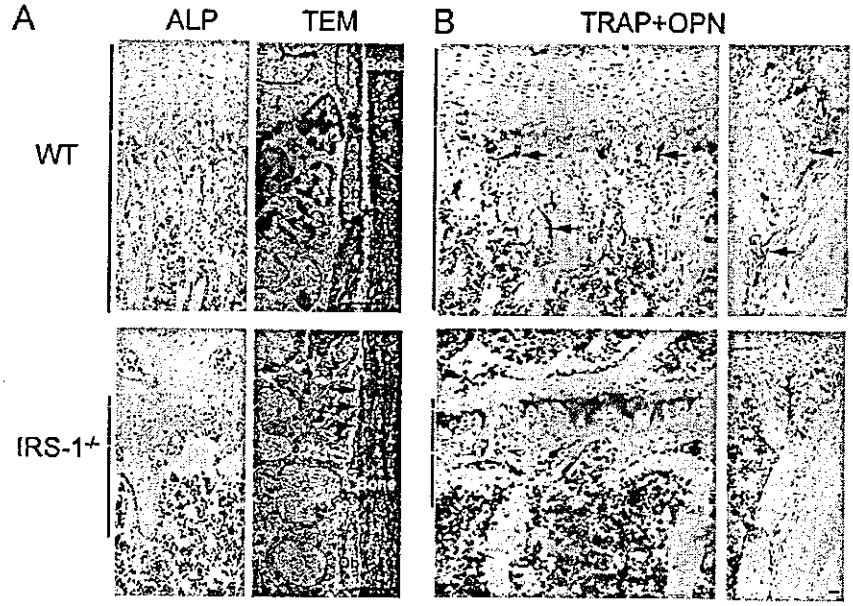

FIG. 5. Histochemical and ultrastructural findings in the primary spongiosa of the proximal tibias of 12-week-old WT and IRS-$1^{-/-}$ mice. Blue, red, and green bars indicate layers of proliferative chondrocytes, hypertrophic chondrocytes, and primary spongiosa, respectively. Bar, 10 μm. (A) Both the volume of primary spongiosa and the number of ALP^+ osteoblasts were decreased in IRS-$1^{-/-}$ mice (left). In the ultrastructural findings by TEM, unmineralized osteoid (asterisk) produced by osteoblasts (Ob) are indicated by green covered the bone surface in WT, while IRS-$1^{-/-}$ osteoblasts were flattened and scarce and were directly attached to the mineralized bone surface (arrows). (B) Double staining of TRACP and osteopontin. $TRACP^+$ osteoclasts (arrows) were rarely seen in the IRS-$1^{-/-}$ primary spongiosa. Osteopontin-positive calcified matrix at the hypertrophic zone was increased (left); however, the cement line of bone collar was decreased (right), suggesting the suppression of bone turnover in IRS-$1^{-/-}$ mice.

that these two molecules are expressed in bone, although they play distinct roles, both of which are important in the regulation of bone metabolism.[24,25] In the epiphyseal cartilage, however, IRS-2 was not expressed, whereas IRS-1 was localized in various types of chondrocytes. In fact, IRS-$2^{-/-}$ mice did not show growth retardation but IRS-$1^{-/-}$ mice did,[26–29] indicating that IRS-2 is much less important than IRS-1 in the epiphyseal cartilage.

Because IGF-I is known to be a potent regulator of chondrocyte metabolism, and its receptor was widely localized in the epiphyseal cartilage, it is most probable that the abnormality seen in the IRS-$1^{-/-}$ cartilage may be caused by the lack of IGF-I signaling acting as an autocrine/paracrine factor. However, our previous study has shown that serum IGF-I levels were similar between WT and IRS-$1^{-/-}$ mice, suggesting the absence of systemic compensation for impaired IGF-I bioactivity.[24] Part of the impairment of the IRS-$1^{-/-}$ epiphyseal cartilage might possibly lie in the role that IGF-I plays in the mechanism by which a number of other hormones act on bone. Growth hormone is a well-known stimulus of IGF-I production in a variety of tissues including cartilage and bone, and it exerts its effects mainly through IGF-I mediation.[38] It is therefore possible that the inhibition of growth hormone signaling through IGF-I production contributes to the growth retardation of IRS-$1^{-/-}$ mice. Similarly, other hormones with effects on cartilage such as sex hormones,[39,40] thyroid hormone,[41] and cortisol[42] alter IGF-I levels in a manner consistent with IGF-I having a role in the actions of these hormones.

To understand the physiological role of IRS-1, it is noteworthy that mice deficient in IGF-I receptor (IGF-IR) and IGF-I exhibit more severe growth retardation than do IRS-$1^{-/-}$ mice.[6,7,28] IGF-$IR^{-/-}$ mice invariably die at birth and show about 45% of the WT body weight,[7] whereas that shown by IRS-$1^{-/-}$ mice was around 60% at birth.[28] IGF-$I^{-/-}$ mice also exhibit more severe growth retardation than IRS-$1^{-/-}$ mice (30% and 60%, respectively, of WT body weight at 8 weeks).[6,28] More importantly, the closure of the epiphyseal cartilage is delayed in IGF-$I^{-/-}$ mice,[6] and it is accelerated in IRS-$1^{-/-}$ mice. These discrepancies may be because of the existence of downstream signaling pathways of IGF-I/IGF-IR other than IRS-1. In fact, the p66 isoform of Shc ($p66^{shc}$) is known to be another adaptor protein that is phosphorylated by the IGF-IR activation. The $p66^{shc}$, which is confirmed to be expressed in chondrocytes and osteoblasts,[43,44] is a signaling molecule that positively regulates apoptosis.[45] It is therefore possible that the decrease in the apoptotic pathway through $p66^{shc}$ causes the delay of the epiphyseal closure in the IGF-$I^{-/-}$ mice, whereas the comparative upregulation of the $p66^{shc}$ sig-

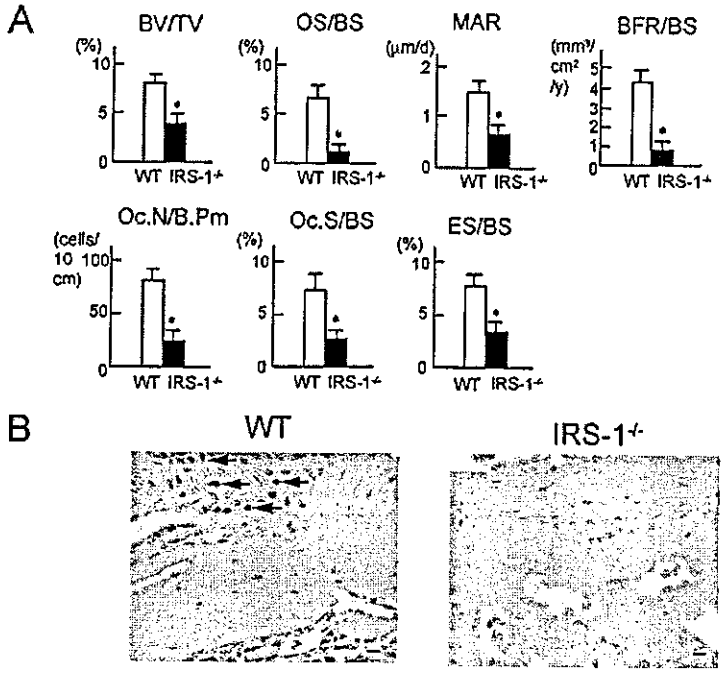

FIG. 6. Histomorphometrical and PCNA immunohistochemical findings in the primary spongiosa of the proximal tibias of 12-week-old WT and IRS-1$^{-/-}$ mice. (A) Histomorphometrical analysis. Parameters were measured in an area 1.2 mm in length from 0.1 mm below the epiphyseal cartilage at the proximal metaphysis of the tibias in Villanueva-Goldner and calcein double-labeled sections. Data are expressed as means (bars) ± SD (error bars) for 6 bones/group for WT and IRS-1$^{-/-}$. *$p < 0.01$ vs. WT. BV/TV, trabecular bone volume expressed as percentage of total tissue volume; OS/BS, percentage of osteoid surface; MAR, mineral apposition rate; BFR/BS, bone formation rate expressed by MAR × percentage of bone exhibiting double labels plus one-half single labels; Oc.N/B.Pm, number of mature osteoclasts in 10 cm of bone perimeter; Oc.S/BS, percentage of bone surface covered by mature osteoclasts; ES/BS, percentage of eroded surface. (B) Immunolocalizations of PCNA. Some osteoblastic cells were positive for PCNA (arrows) in the WT proximal tibias, but they were hardly seen in IRS-1$^{-/-}$. Bar, 10 μm.

naling might lead to apoptosis of the hypertrophic chondrocytes in IRS-1$^{-/-}$ mice. Furthermore, early closure of the epiphyseal cartilage is clinically seen in the adrenogenital syndrome or precocious puberty, indicating the acceleration of the sex hormone production.[46] Because sex hormones are known to induce IGF-I production in chondrocytes,[39,40] IGF-I is assured to be increased in the cartilage. It seems that the p66^{shc} signaling exceeds the IRS-1 signaling under the pathological conditions. Although the skeletal phenotype of the p66^{shc}-deficient mice has not yet been reported, our next task will be to elucidate the differential regulation of chondrocytes by IRS-1 and p66^{shc} signalings.

In the IRS-1$^{-/-}$ primary spongiosa, both bone formation and resorption were decreased, showing a state of low bone turnover. Histomorphometrical and PCNA immunohistochemical analyses revealed the impairment of osteoblast proliferation (PCNA) and activity (mineral apposition rate). Regarding osteoclastic cells, because we previously reported that IRS-1 is not expressed in these cells, the down-regulation of bone resorption markers is likely to be caused by the decrease in the supporting ability of osteoclastogenesis by osteoblasts through RANKL induction.[24] These abnormalities in the cartilage and bone seen in the IRS-1$^{-/-}$ mice resemble those of skeletal senility in humans.[47] Although the involvement of IRS-1 in human aging is unknown, a reduction in IGF-I is implicated as an important factor in the etiology of age-related bone loss.[48–50] Thus, IRS-1 signaling might be important in the prevention of skeletal ageing caused by the decrease of IGF-I.

Taken together, we hereby conclude that IRS-1 signaling is important for skeletal growth because it prevents the closure of the epiphyseal cartilage and maintains subsequent bone turnover at the primary spongiosa. Because our preliminary study has revealed that IRS-1 deficiency also impairs fracture healing,[51] further studies on IRS-1 signaling in the regulation of cartilage and bone metabolism are anticipated to disclose not only the molecular mechanism of skeletal growth and aging, but also that of pathological conditions such as osteoarthritis and osteoporosis.

ACKNOWLEDGMENTS

This study was supported by Grants-in-Aid for Scientific Research from the Japanese Ministry of Education, Culture, Sports, Science and Technology (11470301 and 12137201), the Uehara Memorial Foundation, the Takeda Science Foundation, and the Nakatomi Memorial Foundation.

REFERENCES

1. Thomas D, Hards D, Rogers S, Ng K, Best J 1997 Insulin and bone, clinical and scientific view. Endocrinol Metab Clin North Am 4:5–17.
2. Canalis E 1993 Insulin like growth factors and the local regulation of bone formation. Bone 14:273–276.
3. Laron Z 2001 Insulin-like growth factor 1 (IGF-1): A growth hormone. Mol Pathol 54:311–316.
4. Chihara K, Sugimoto T 1997 The action of GH/IGF-I/IGFBP in osteoblasts and osteoclasts. Horm Res 48(Suppl 5):45–49.
5. Hayden JM, Mohan S, Baylink DJ 1995 The insulin-like growth factor system and the coupling of formation to resorption. Bone 17(Suppl 2):93S–98S.
6. Baker J, Liu JP, Robertson EJ, Efstratiadis A 1993 Role of insulin-like growth factors in embryonic and postnatal growth. Cell 75: 73–82.

7. Liu JP, Baker J, Perkins AS, Robertson EJ, Efstratiadis A 1993 Mice carrying null mutations of the genes encoding insulin-like growth factor I (Igf-1) and type 1 IGF receptor (Igf1r). Cell 75:59–72.
8. Laron Z, Klinger B, Silbergeld A 1999 Patients with Laron syndrome have osteopenia/osteoporosis. J Bone Miner Res 14:156–157.
9. Shen FH, Visger JM, Balian G, Hurwitz SR, Diduch DR 2002 Systemically administered mesenchymal stromal cells transduced with insulin-like growth factor-I localize to a fracture site and potentiate healing. J Orthop Trauma 16:651–659.
10. Trippel SB 1998 Potential role of insulin like growth factors in fracture healing. Clin Orthop 355(Suppl):S301–S313.
11. Andrew JG, Hoyland J, Freemont AJ, Marsh D 1993 Insulinlike growth factor gene expression in human fracture callus. Calcif Tissue Int 53:97–102.
12. Schmidmaier G, Wildemann B, Heeger J, Gabelein T, Flyvbjerg A, Bail HJ, Raschke M 2002 Improvement of fracture healing by systemic administration of growth hormone and local application of insulin-like growth factor-1 and transforming growth factor-beta1. Bone 31:165–172.
13. Shukunami C, Shigeno C, Atsumi T, Ishizeki K, Suzuki F, Hiraki Y 1996 Chondrogenic differentiation of clonal mouse embryonic cell line ATDC5 in vitro: Differentiation-dependent gene expression of parathyroid hormone (PTH)/PTH-related peptide receptor. J Cell Biol 133:457–468.
14. Kato Y, Gospodarowicz D 1984 Growth requirements of low-density rabbit costal chondrocyte cultures maintained in serum-free medium. J Cell Physiol 120:354–363.
15. Krakauer JC, McKenna MJ, Rao DS, Whitehouse FW 1997 Bone mineral density in diabetes. Diabetes Care 20:1339–1340.
16. Piepkorn B, Kann P, Forst T, Andreas J, Pfutzner A, Beyer J 1997 Bone mineral density and bone metabolism in diabetes mellitus. Horm Metab Res 29:584–591.
17. Kawaguchi H, Kurokawa T, Hanada K, Hiyama Y, Tamura M, Ogata E, Matsumoto T 1994 Stimulation of fracture repair by recombinant human basic fibroblast growth factor in normal and streptozotocin-diabetic rats. Endocrinology 135:774–781.
18. Funk JR, Hale JE, Carmines D, Gooch HL, Hurwitz SR 2000 Biomechanical evaluation of early fracture healing in normal and diabetic rats. J Orthop Res 18:126–132.
19. Loder RT 1988 The influence of diabetes mellitus on the healing of closed fractures. Clin Orthop 232:210–216.
20. Burks DJ, White MF 2001 IRS proteins and beta-cell function. Diabetes 50(Suppl 1):S140–S145.
21. Kadowaki T, Tobe K, Honda-Yamamoto R, Tamemoto H, Kaburagi Y, Momomura K, Ueki K, Takahashi Y, Yamauchi T, Akanuma Y, Yazaki Y 1996 Signal transduction mechanism of insulin and insulin-like growth factor-1. Endocr J 43(Suppl):S33–S41.
22. Lavan BE, Lane WS, Lienhard GE 1997 The 60-kDa phosphotyrosine protein in insulin-treated adipocytes is a new member of the insulin receptor substrate family. J Biol Chem 272:11439–11443.
23. Lavan BE, Fantin VR, Chang ET, Lane WS, Keller SR, Lienhard GE 1997 A novel 160-kDa phosphotyrosine protein in insulin-treated embryonic kidney cells is a new member of the insulin receptor substrate family. J Biol Chem 272:21403–21407.
24. Ogata N, Chikazu D, Kubota N, Terauchi Y, Tobe K, Azuma Y, Ohta T, Kadowaki T, Nakamura K, Kawaguchi H 2000 Insulin receptor substrate-1 in osteoblast is indispensable for maintaining bone turnover. J Clin Invest 105:935–943.
25. Akune T, Ogata N, Hoshi K, Kubota N, Terauchi Y, Tobe K, Takagi H, Azuma Y, Kadowaki T, Nakamura K, Kawaguchi H 2002 Insulin receptor substrate-2 maintains predominance of anabolic function over catabolic function of osteoblasts. J Cell Biol 159:147–156.
26. Tamemoto H, Kadowaki T, Tobe K, Yagi T, Sakura H, Hayakawa T, Terauchi Y, Ueki K, Kaburagi Y, Satoh S, Sekihara H, Yoshioka S, Horikoshi H, Furuta Y, Ikawa Y, Kasuga M, Yazaki Y, Aizawa S 1994 Insulin resistance and growth retardation in mice lacking insulin receptor substrate-1. Nature 372:182–186.
27. Kubota N, Tobe K, Terauchi Y, Eto K, Yamauchi T, Suzuki R, Tsubamoto Y, Komeda K, Nakano R, Miki H, Satoh S, Sekihara H, Sciacchitano S, Lesniak M, Aizawa S, Nagai R, Kimura S, Akanuma Y, Taylor SI, Kadowaki T 2000 Disruption of insulin receptor substrate 2 causes type 2 diabetes because of liver insulin resistance and lack of compensatory beta-cell hyperplasia. Diabetes 49:1880–1889.
28. Araki E, Lipes MA, Patti ME, Bruning JC, Haag B III, Johnson RS, Kahn CR 1994 Alternative pathway of insulin signalling in mice with targeted disruption of the IRS-1 gene. Nature 372:186–190.
29. Withers DJ, Gutierrez JS, Towery H, Burks DJ, Ren JM, Previs S, Zhang Y, Bernal D, Pons S, Shulman GI, Bonner-Weir S, White MF 1998 Disruption of IRS-2 causes type 2 diabetes in mice. Nature 391:900–904.
30. Hoshi K, Komori T, Ozawa H 1999 Morphological characterization of skeletal cells in Cbfa1-deficient mice. Bone 25:639–651.
31. Amizuka N, Henderson JE, Hoshi K, Warshawsky H, Ozawa H, Goltzman D, Karaplis AC 1996 Programmed cell death of chondrocytes and aberrant chondrogenesis in mice homozygous for parathyroid hormone-related peptide gene deletion. Endocrinology 137:5055–5067.
32. Ito M, Amizuka N, Nakajima T, Ozawa H 1999 Ultrastructural and cytochemical studies on cell death of osteoclasts induced by bisphosphonate treatment. Bone 25:447–452.
33. Karaplis AC 2002 Embryonic development of bone and the molecular regulation of intramembranous and endochondral bone formation. In: Bilezikian JP, Raisz LG, Rodan GA (eds.) Principles of Bone Biology, 2nd ed., vol. 1. Academic Press, San Diego, CA, USA, pp. 33–58.
34. Hoshi K, Ejiri S, Ozawa H 2001 Organic components of crystal sheaths in bones. J Electron Microsc (Tokyo) 50:33–40.
35. McKee MD, Nanci A 1996 Osteopontin: An interfacial extracellular matrix protein in mineralized tissues. Connect Tissue Res 35:197–205.
36. Bruning JC, Winnay J, Cheatham B, Kahn CR 1997 Differential signaling by insulin receptor substrate 1 (IRS-1) and IRS-2 in IRS-1-deficient cells. Mol Cell Biol 17:1513–1521.
37. Yamauchi T, Tobe K, Tamemoto H, Ueki K, Kaburagi Y, Yamamoto-Honda R, Takahashi Y, Yoshizawa F, Aizawa S, Akanuma Y, Sonenberg N, Yazaki Y, Kadowaki T 1996 Insulin signalling and insulin actions in the muscles and livers of insulin-resistant, insulin receptor substrate 1-deficient mice. Mol Cell Biol 16:3074–3084.
38. Ohlsson C, Bengtsson BA, Isaksson OG, Andreassen TT, Slootweg MC 1998 Growth hormone and bone. Endocr Rev 19:55–79.
39. Maor G, Segev Y, Phillip M 1999 Testosterone stimulates insulin-like growth factor-I and insulin-like growth factor-I-receptor gene expression in the mandibular condyle–a model of endochondral ossification. Endocrinology 140:1901–1910.
40. Gori F, Hofbauer LC, Conover CA, Khosla S 1999 Effects of androgens on the insulin-like growth factor system in an androgen-responsive human osteoblastic cell line. Endocrinology 140:5579–5586.
41. Huang BK, Golden LA, Tarjan G, Madison LD, Stern PH 2000 Insulin-like growth factor I production is essential for anabolic effects of thyroid hormone in osteoblasts. J Bone Miner Res 15:188–197.
42. McCarthy TL, Centrella M, Canalis E 1990 Cortisol inhibits the synthesis of insulin-like growth factor-I in skeletal cells. Endocrinology 126:1569–1575.
43. Shakibaei M, John T, De Souza P, Rahmanzadeh R, Merker HJ 1999 Signal transduction by beta1 integrin receptors in human chondrocytes in vitro: Collaboration with the insulin-like growth factor-I receptor. Biochem J 342:615–623.
44. Caverzasio J, Palmer G, Suzuki A, Bonjour JP 1997 Mechanism of the mitogenic effect of fluoride on osteoblast-like cells: Evidences for a G protein-dependent tyrosine phosphorylation process. J Bone Miner Res 12:1975–1983.
45. Migliaccio E, Giorgio M, Mele S, Pelicci G, Reboldi P, Pandolfi PP, Lanfrancone L, Pelicci PG 1999 The p66shc adaptor protein controls oxidative stress response and life span in mammals. Nature 402:309–313.
46. Aldegheri R 1999 Distraction osteogenesis for lengthening of the tibia in patients who have limb-length discrepancy or short stature. J Bone Joint Surg Am 81:624–634.
47. Marcus R 1996 The nature of osteoporosis. In: Marcus R, Feldman D, Kelsey J (eds.) Osteoporosis. Academic Press, San Diego, CA, USA, pp. 647–660.

48. Canalis E 1997 Insulin-like growth factors and osteoporosis. Bone 21:215–216.
49. Nicolas V, Prewett A, Bettica P, Mohan S, Finkelman RD, Baylink DJ, Farley JR 1994 Age-related decreases in insulin-like growth factor-I and transforming growth factor-beta in femoral cortical bone from both men and women: Implications for bone loss with aging. J Clin Endocrinol Metab 78:1011–1016.
50. Rosen CJ 1994 Growth hormone, insulin-like growth factors, and the senescent skeleton: Ponce de Leon's fountain revisited? J Cell Biochem 56:348–356.
51. Shimoaka T, Hoshi K, Kadowaki T, Terauchi Y, Nakamura K, Kawaguchi H 2001 Insulin receptor substrate-1 (IRS-1) is essential for bone repair through stimulation of cell proliferation at its early stage. J Bone Miner Res 16:S1;S181.

Address reprint requests to:
Kazuto Hoshi, MD, PhD
Department of MENICON Cartilage and Bone Regeneration
Faculty of Medicine
University of Tokyo
Hongo 7-3-1
Bunkyo, Tokyo 113-8655, Japan
E-mail: pochi-tky@umin.ac.jp

Received in original form March 17, 2003; in revised form July 9, 2003; accepted September 10, 2003.

THE JOURNAL OF GENE MEDICINE
J Gene Med 2004; 6: 76–84.
Published online in Wiley InterScience (www.interscience.wiley.com). DOI: 10.1002/jgm.470

RESEARCH ARTICLE

In situ single cell observation by fluorescence resonance energy transfer reveals fast intra-cytoplasmic delivery and easy release of plasmid DNA complexed with linear polyethylenimine

Keiji Itaka[1,2]
Atsushi Harada[1]
Yuichi Yamasaki[1]
Kozo Nakamura[2]
Hiroshi Kawaguchi[2]
Kazunori Kataoka[1]*

[1]*Department of Materials Science and Engineering, Graduate School of Engineering, The University of Tokyo, 7-3-1 Hongo, Bunkyo-ku, Tokyo 113-8656, Japan*

[2]*Department of Orthopaedic Surgery, Faculty of Medicine, The University of Tokyo, 7-3-1 Hongo, Bunkyo-ku, Tokyo 113- 8655, Japan*

*Correspondence to:
Professor Kazunori Kataoka, Department of Materials Science and Engineering, Graduate School of Engineering, The University of Tokyo, 7-3-1 Hongo, Bunkyo-ku, Tokyo 113-8656, Japan.
E-mail:
kataoka@bmw.t.u-tokyo.ac.jp

Received: 9 May 2003
Revised: 11 July 2003
Accepted: 11 July 2003

Abstract

Background The investigation into the intracellular mechanisms for gene expression has acquired great impetus for the improvement of the transfection efficiency by a non-viral gene delivery system.

Methods Intracellular trafficking as well as release of plasmid DNA (pDNA) complexed with polycations, including linear and branched polyethylenimine (LPEI, BPEI) and poly(L-lysine) (PLL), were explored under confocal microscopy using fluorescence resonance energy transfer (FRET) between a pair of donor–acceptor fluorescent dyes (fluorescein and Cy3) tagged on a single pDNA molecule.

Results pDNA complexed with LPEI underwent a rapid escape from the endosomes, spreading uniformly into the cytoplasm with a substantial decrease in FRET efficiency due to the disintegration of LPEI/pDNA polyplex structure. pDNA complexed with BPEI also achieved a rapid escape from the endosomes. Nevertheless, the pDNA retained high FRET efficiency even after 24 h, indicating an appreciable stability of the BPEI/pDNA polyplex to keep pDNA in a condensed state. In the PLL/pDNA polyplexes, neither endosome escape nor pDNA decondensation was observed. These intracellular characteristics of polyplexes showed a clear correlation to their gene transfection efficiency: The LPEI/pDNA revealed a considerably higher and faster gene expression compared with BPEI/pDNA. Atomic force microscopy revealed that BPEI induced more effective condensation of pDNA than LPEI, being consistent with restricted cytoplasmic release of complexed pDNA.

Conclusion Fast endosomal escape and subsequent smooth disintegration of LPEI/pDNA in the cytoplasm are likely to be determining factors for the excellent transfection efficiency of this polyplex system. These properties may be particularly beneficial to achieve appreciably high gene expression in a prompt manner. Copyright © 2004 John Wiley & Sons, Ltd.

Keywords polyethylenimine; DNA; fluorescence resonance energy transfer; confocal microscopy; transfection; nucleic acid conformation

Introduction

Improvement of transfection efficiency is one of the most important subjects for the development of a non-viral gene delivery system. For this purpose,

investigations into the intracellular mechanisms for gene expression have been acquiring great importance [1]. Many cationic polymers indeed condense plasmid DNA (pDNA) through an electrostatic interaction, which is a requirement for effective cellular uptake [2,3]. However, sufficient transfection efficiency for clinical application has not been achieved, probably due to barriers such as endosomal degradation of pDNA or the limitation of nuclear localization. In recent years, special attention has been directed toward polyethylenimine (PEI), which has shown excellent gene expression compared with other polymers such as poly(L-lysine) (PLL). The mechanisms are usually explained by the 'proton-sponge' effect based on the uniqueness of the chemical structure of PEI [4,5]. Due to the integrated amino groups in the backbone structure, PEI possesses a low pKa to show a buffering property below physiological pH. Thus, PEI in the endosome interferes with pH lowering of the compartment, and induces an increased ion osmotic pressure to cause endosomal swelling and subsequent disruption [6]. Consequently, the endocytosed PEI polyplex can be efficiently delivered into the cytoplasm.

Two different structures of PEI, i.e., linear and branched PEI, have so far been applied to construct polyplex systems. Initially, appreciable gene expressions without using chloroquine were often reported for polyplexes composed of 800 and 25 kDa branched PEI (BPEI) [4,5,7–10], yet recent studies revealed that the 22 kDa linear PEI (LPEI) has even higher transfection activity [11–17]. Although BPEI and LPEI have identical chemical formulas, their buffering capacities are not considered comparable because of the difference in the amine composition: The amines present in LPEI are all secondary, in contrast, of those in BPEI, 25, 50, and 25% are primary, secondary, and tertiary, respectively [18]. Based on the studies comparing various LPEI and BPEI samples with a broad range of molecular weight, there were indeed observed significant differences in the transfection efficiencies [19,20]. Nevertheless, it is still unsolved whether the different efficiencies of the PEI family can simply be explained from the standpoint of the 'proton-sponge' effect, motivating us to conduct the present study to explore the intracellular behavior of PEI/pDNA polyplexes with varying composition.

Herein, we observed the intracellular fate of the internalized polyplexes by microscopic observation using fluorescently labeled pDNA. By using doubly labeled pDNA with a pair of donor–acceptor fluorescent dyes (fluorescein and Cy3), the condensation state of pDNA inside the cells was clearly detected by fluorescence resonance energy transfer (FRET) measurement. Moreover, the structural properties of the PEI/pDNA polyplexes, which might correlate with their intracellular kinetics, were analyzed by atomic force microscopy (AFM). Notably, in the LPEI/pDNA polyplexes, rapid escape from the endosomes, effective release of pDNA from the complex into the cytoplasm, and easy pDNA decondensation were observed in a sequential manner, correlating with the excellent and earlier detectable gene expression.

Materials and methods

Materials

Branched polyethylenimine (BPEI, MW 25 kDa) was purchased from Aldrich Chemical Co. (USA). Linear polyethylenimine (LPEI, MW 22 kDa) was purchased from MBI Fermentas (Exgen 500; Germany). Poly(L-lysine) (PLL, MW 53 900) and poly(aspartic acid) sodium salt (MW 26 000) were purchased from Sigma (St. Louis, MO, USA). The pDNA encoding luciferase (pGL3-Luc, Promega, USA; 5256 bps) was amplified in competent DH5α *Escherichia coli* and purified using EndoFree™ Plasmid Maxi Kits (Qiagen GmbH, Germany). The DNA concentration was determined by the absorbance at 260 nm. Dulbecco's modified Eagle's medium (DMEM) and fetal bovine serum (FBS) were purchased from Sigma. Texas Red Dextran (MW 3000) was purchased from Molecular Probes (Eugene, OR, USA). Hoechst 33258 was purchased from Dojindo (Japan).

Fluorescent labeling

The plasmid DNA (pDNA) was labeled in a similar way as that previously described using a Label IT nucleic acid labeling kit (Panvera, USA) [21]. Following a protocol provided by the manufacturer, slightly modified to allow double labeling of DNA, 5–50 μl of a pDNA solution (1 mg/ml) and the same amount of Label IT reagent (for fluorescein, Cy3 and X-rhodamine) were mixed in 20 mM MOPS buffer (pH 7.5) and incubated at 37 °C for 2 h. For double labeling, the two reagents (fluorescein + Cy3 or fluorescein + X-rhodamine) were simultaneously added to the pDNA solution. Any unreacted labeling reagent was removed and pDNA was purified by ethanol precipitation.

Preparation of polyplexes

The polycations and pDNA were separately dissolved in 10 mM Tris-HCl buffer (pH 7.4). Both solutions were mixed at various charge ratios of the number of nitrogen atoms to DNA phosphates. The final DNA concentration was adjusted to 33.3 μg/ml. After 15 min of incubation, the mixture was used for transfection and other measurements.

In vitro transfection

293T cells were seeded in 24-well culture plates. After a 24-h incubation in medium containing 10% FBS, the cells were rinsed and then 250 μl of culture medium without FBS were added to each well. Polyplex solution (25 μl; the pDNA concentration was 30μg/ml) was applied to each well. After 4 h, the medium was removed and replaced by 10% FBS containing medium for further incubation. The luciferase gene expression was measured using Fluoroscan Ascent FL (Dainippon, Japan).

Flow cytometric analysis

The polyplexes loaded with fluorescein-labeled pDNA were applied to the 293T cells in a manner similar to the procedure for *in vitro* transfection. After a 1-h incubation, the culture medium was aspirated and the cells were washed twice with phosphate-buffered saline (PBS). After detachment by pipetting and resuspension in PBS, the cells were analyzed using a flow cytometer (EPICS XL, Beckman Coulter, Inc.). Mock transfection allowed the definition of the natural fluorescence limit for the 293T cells and thus assessment of the fluorescein-positive cells. The cytometric data were analyzed using EXPO32™ software (Beckman Coulter, Inc.).

Laser confocal microscopy

The cells were seeded in 35-mm glass base dishes (Iwaki, Japan) for laser confocal analysis. A LSM 510 laser scanning microscope, set up from an Axiovert 100M microscope (Carl Zeiss, Germany), was used for the optical sectioning of the cells. An argon/krypton mixed gas laser with an excitation wavelength at 488 nm was used to induce emission from fluorescein and Cy3. For observation of the nuclei stained by Hoechst 33 258 and the endosomes stained by Texas Red Dextran, excitation wavelengths at 364 nm (Ar laser) and 543 nm (HeNe laser) were used, respectively.

When the pDNA was labeled with only fluorescein, the emission was observed using a 505 nm long pass filter. For analyzing FRET with doubly labeled pDNA, the emissions of fluorescein and Cy3 were detected by a 500–530 nm band pass filter and a 560 nm long pass filter, respectively. The fluorescence intensity ratios were calculated (LSM 510 Software, version 2.02; Carl Zeiss, Germany) at each pixel using the following equation:

$$\text{Fluorescein/Cy3 Ratio} = (S1 - S2)/(S1 + S2) \times 256 + 128$$

where S1 and S2 indicate the emission intensities of fluorescein and Cy3, respectively. The ratio image with an 8-bit (256 levels) gray scale was then created to express the ratios on the cell image.

Exchange reaction assay

The FRET measurements associated with the globule-to-coil transition of pDNA, which is triggered by the dissociation of the polyplexes, were carried out as previously described [21]. The fluorescence emission was measured at 25 °C using a spectrofluorometer (FP-777; JASCO, Japan). The excitation wavelength was 492 nm.

The LPEI, BPEI, and PLL/pDNA polyplexes (DNA concentration was 20 μg/ml) were prepared by using the doubly labeled (fluorescein and X-rhodamine) pDNA. After measurement of the initial emission intensity ratio of X-rhodamine/fluorescein, a 20% volume of poly(aspartic acid) solution (840 μg/ml) was added (the molar ratio of aspartic residue to DNA phosphate was 20), and, with gentle stirring, the time-dependent change in the emission intensity ratio was evaluated.

Atomic force microscopy

Each polyplex sample solution (5 μl) was deposited on a freshly cleaved mica substrate for 30 s. The solution was then rinsed with 50 μl of MilliQ deionized water (Millipore) and dried under a gentle flow of nitrogen gas. AFM imaging was performed in the tapping mode with standard silicon probes (Olympus, Tokyo, Japan) on a NVB100 microscope (Olympus) controlled by Nanoscope IIIa software (Digital Instruments, USA). The cantilever oscillation frequency was tuned to the resonance frequency of the cantilever, 260–340 kHz. The 256 × 256 images were recorded at a 0.5–2 μm/s linear scanning speed at a sampling density of 4–60 nm^2 per pixel. The raw AFM images were processed only for background removal (flattening) using the software.

Results

N/P ratio of cationic polymer/pDNA polyplexes

The polyplexes of the cationic polymers and pDNA at various N/P ratios (N/P = 1–20) were tested for transfection to 293T cells. The best transfection efficiencies were obtained for N/P = 10 in LPEI and BPEI, and N/P = 2 in PLL (data not shown). The gene expression obtained by LPEI was 10–100 times greater than BPEI (see Figure 6, discussed later). These N/P ratios were then used when preparing each polyplex throughout this study.

Transfer of the polyplexes from endosomes to the cytoplasm

The first step in the transfection is the cellular association and internalization of the polyplexes. By using the fluorescein-labeled pDNA, the cellular uptake of the polyplexes (LPEI, BPEI, and PLL/pDNA) was investigated. From flow cytometric analysis, the fluorescein-positive cells were estimated to be more than 90% even after a 1-h incubation with each polyplex, indicating that considerable association of these polyplexes and cells was achieved. The internalization of the polyplexes was then observed using laser confocal microscopy. To certify the escape from the endosomes, Texas Red Dextran was used as the endosome marker. After a 4-h incubation with either the LPEI/pDNA or the BPEI/pDNA polyplex, signals of fluorescein and Texas Red were separately observed in the cytoplasm (Figure 1), indicating that the polyplexes had already escaped from the endosomes. On the other

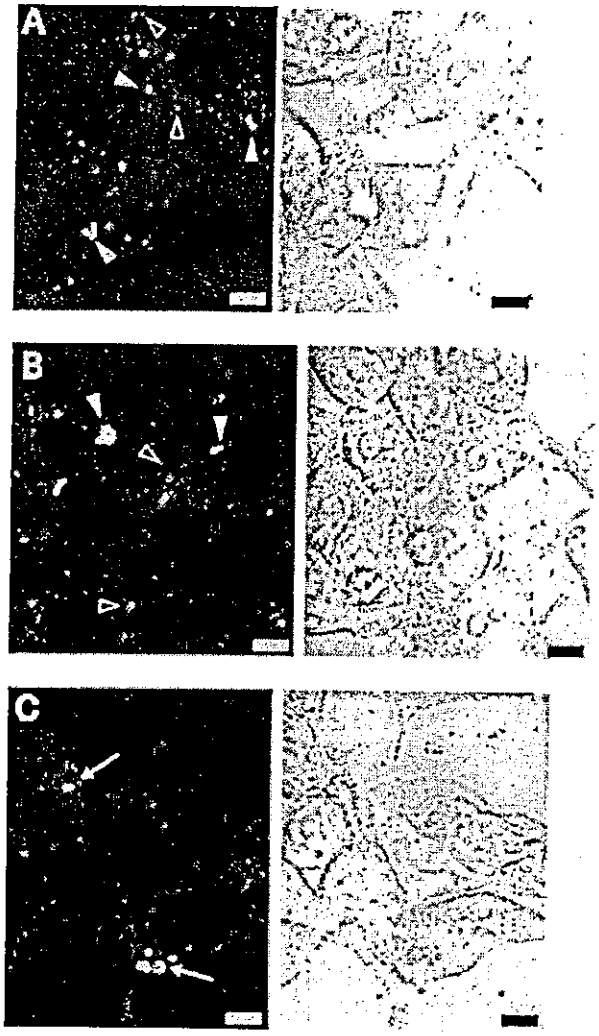

Figure 1. Transfer of the polyplexes from endosomes to the cytoplasm. The polyplexes were formed by polycations (LPEI, BPEI, and PLL) and fluorescein-labeled pDNA. 293T cells were seeded in 24-well culture plates. After a 24-h incubation in medium containing 10% FBS, the cells were rinsed and then 250 μl of culture medium without FBS were added to each well. The polyplex solution (25 μl; pDNA concentration was 30 μg/ml) was applied to each well. After a 4-h incubation, confocal microscopic images were obtained with endosome staining by Texas Red Dextran. The fluorescent images are shown on the left-hand side and the corresponding phase contrast images are on the right. (A) LPEI/pDNA and (B) BPEI/pDNA. DNA complexes (arrowhead) and dextran (open arrowhead) were separately observed. (C) PLL/pDNA. DNA complex and dextran were co-localized (observed as yellowish spot). Bar: 10 μm

hand, in the PLL/pDNA polyplexes, both the fluorescein and Texas Red signals were co-localized (observed as yellowish spot in Figure 1), even after 4 h.

It has been reported in the literature that the escape of BPEI/pDNA polyplexes from the endosomes occurs within 4 h after transfection based on an experiment using a proton pump inhibitor that prevented acidification of the endosomes [22]. In this study, both LPEI and BPEI were observed to escape from the endosomes after 4 h, presumably suggesting a similar endosomolytic activity of PEI by the proton-sponge effect.

Observation of pDNA decondensation in the cytoplasm

The next step for gene expression is pDNA release into the cytoplasm and transportation to the nucleus. After 24 h of transfection with the fluorescein-labeled pDNA, the microscopic images showed remarkable differences among the polyplexes. In LPEI/pDNA, the fluorescein signals were spread all around the cytoplasm (Figure 2). In contrast, the BPEI/pDNA polyplex was also distributed in the cytoplasm; however, it remained dot-shaped, similar to that observed after 1 h of transfection. This result suggested a difference in the polyplex structures.

For further investigation, the doubly labeled pDNA was used for FRET analysis. As previously reported, the condensation of the doubly labeled (fluorescein and X-rhodamine) pDNA in the polyplex induced FRET between the two fluorescent molecules, and the condensation state

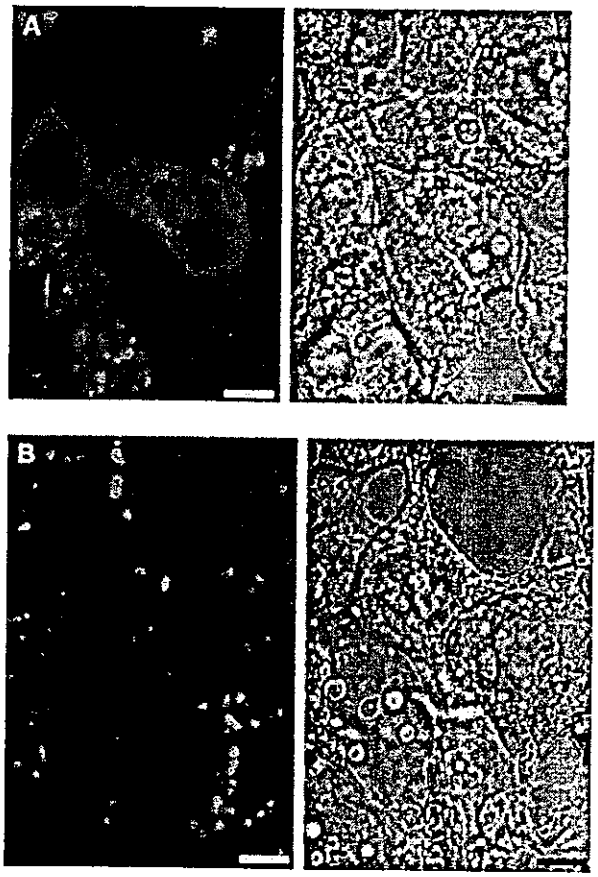

Figure 2. Intracellular distribution of fluorescein-labeled pDNA after 24 h of transfection. The polyplexes loaded with fluorescein-labeled pDNA were applied to the 293T cells. After a 24-h incubation, confocal microscopic images were obtained. The corresponding phase contrast images are on the right. (A) LPEI/pDNA and (B) BPEI/pDNA. Bar 10 μm

of pDNA can be evaluated even under physiological conditions [21]. In this study, fluorescein and Cy3 were used for double labeling. By spectral analysis with excitation at 492 nm, fluorescein (520 nm) has higher intensity than Cy3 (570 nm) in free pDNA. In contrast, when pDNA took a condensed state through complexation with the polycation, the emission peak of Cy3 significantly increased due to FRET from fluorescein, with a concomitant decrease in peak intensity of fluorescein (data not shown).

By using this doubly labeled pDNA, the intracellular distribution of polyplexes was analyzed by FRET under laser confocal microscopy. As shown in Figure 3, the cells transfected by the LPEI/pDNA polyplexes were observed with diffuse distribution of white-colored (higher value of the fluorescein/Cy3 ratio) pDNA in the cytoplasm. This higher fluorescein/Cy3 ratio compared with the background indicated that the emission intensity of fluorescein had higher emission intensity than Cy3 (S1 > S2; see 'Methods'), thus the pDNA acheived a decondensed state where FRET did not occur. In contrast, the cells transfected by the BPEI/pDNA polyplexes were observed as black-colored (lower fluorescein/Cy3 ratio; S1 < S2) and dotted particles, in which the pDNA remained in the condensed state (Figure 3). The result obtained by the PLL/pDNA polyplexes also indicated a similar condensation state. However, the number of polyplexes observed in the cytoplasm was extremely small, even lower compared with that observed after 4 h of transfection.

The DNA decondensation should be necessary to accomplish transcription to mRNA. The feasibility of the pDNA decondensation is thus believed to be closely correlated to the transfection efficiency. To confirm this hypothesis, the time-dependent increase in the pDNA decondensation and the gene expression was evaluated. In the LPEI/pDNA polyplexes, the intracellular decondensation of pDNA was observed within 4 h after transfection, and the amount of decondensed pDNA increased in a time-dependent manner (Figure 4). Concomitantly, the luciferase gene expression was confirmed as quickly as 4 h after transfection, and showed a time-dependent increase (Figure 5), thus presenting a clear correlation with the pDNA decondensation. In contrast, the gene expression by BPEI/pDNA was hardly observed after 4 h, which is consistent with the restricted pDNA decondensation, and, even after a 24-h incubation, only 1/50 to 1/100 of the gene expression was obtained.

It should be noted that pDNA transportation to the nucleus, where the transcription is considered to occur, was not clearly observed for any cases. As shown in Figures 3A and 4, the nucleus was observed as a 'punched-out' shape in the cell. After staining the nucleus with Hoechst 33 258, the localization of the fluorescein-labeled pDNA at the nucleus was rarely detected in each polyplex (Figure 6). Thus, there was a strong indication that only a small portion of the internalized pDNA had been transported to the nucleus. This issue may be related to the intracellular mobility of the polyplexes, and will be discussed below.

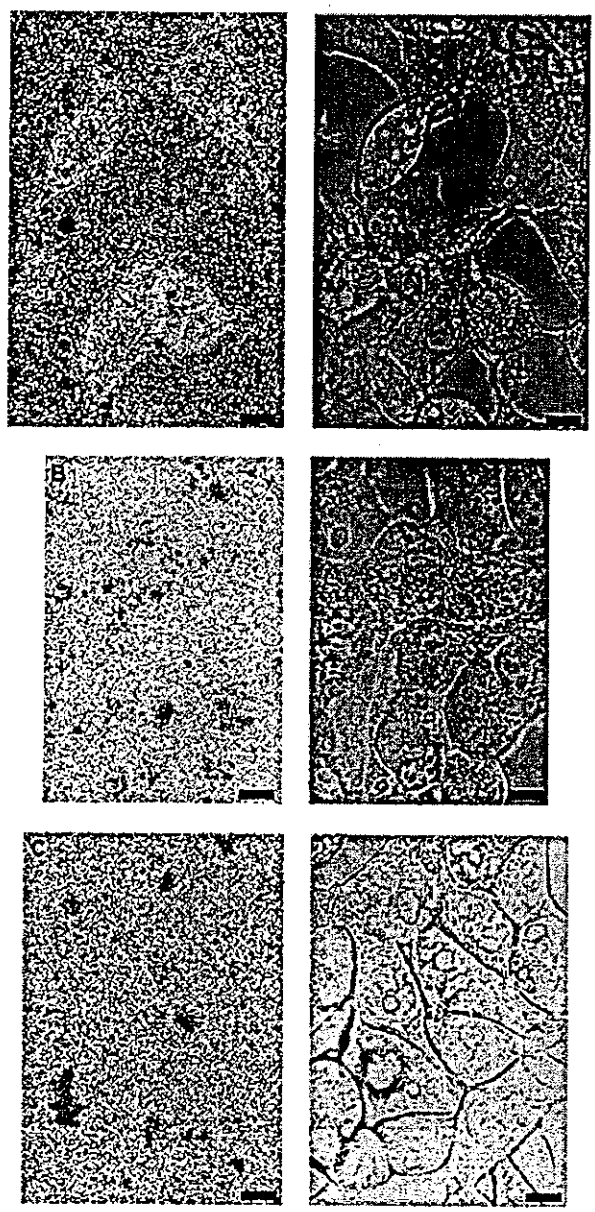

Figure 3. Polyplex distribution after 24 h of transfection expressed by the ratio images. The polyplexes loaded with doubly labeled (fluorescein and Cy3) pDNA were used. For analyzing FRET, the emissions of fluorescein and Cy3 were detected by a 500–530 nm band pass filter and a 560 nm long pass filter, respectively. The fluorescence intensity ratios were calculated at each pixel using LSM 510 Software version 2.02 (Carl Zeiss, Germany, see 'Methods'), and the ratio image with an 8-bit (256 levels) gray scale was then created to express the ratios on the cell image. The corresponding phase contrast images are on the right. (A) LPEI/pDNA; (B) BPEI/pDNA; and (C) PLL/pDNA. Bar 10 μm

Feasibility of the pDNA release from the polyplexes

The decondensation of pDNA is induced after pDNA dissociation from the polycation. Inside the cells, the

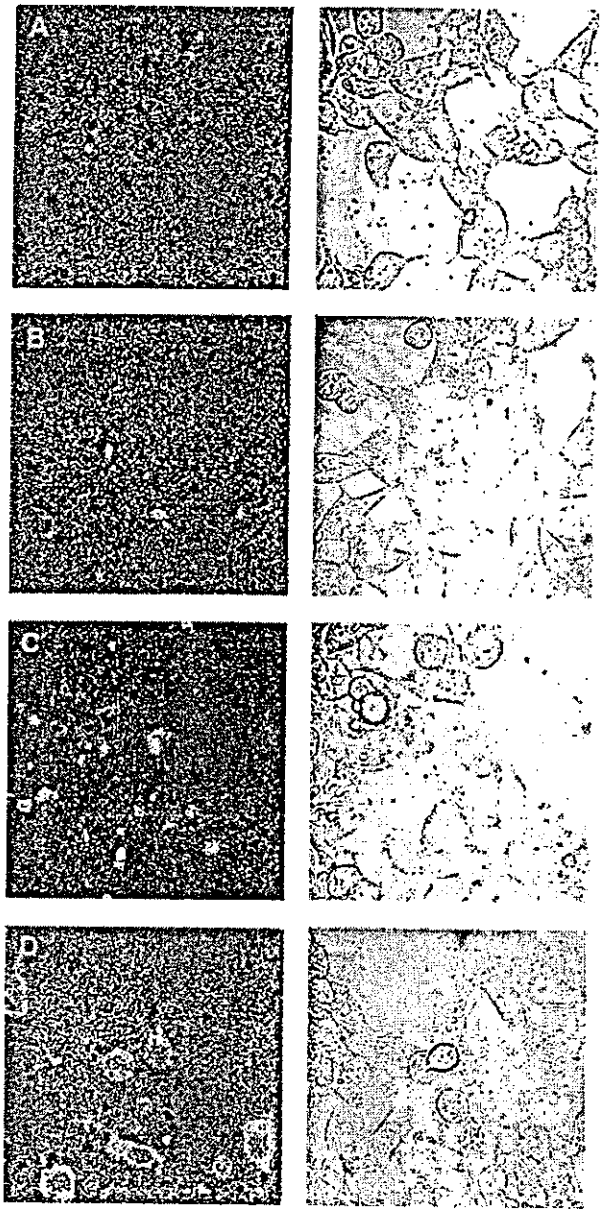

Figure 4. Time-dependent increase of decondensed pDNA after transfection with LPEI/pDNA polyplexes. The ratio images were created after transfection by LPEI/doubly labeled (fluorescein and Cy3) pDNA. The cells were observed with a diffuse distribution of white-colored (higher value of the fluorescein/Cy3 ratio) pDNA in the cytoplasm. This higher fluorescein/Cy3 ratio compared with the background indicated that the emission intensity of fluorescein had higher emission intensity than Cy3 (S1 > S2; see 'Methods'), thus the pDNA took a decondensed state where FRET did not occur. The corresponding phase contrast images are on the right. The ratio image after (A) 4 h; (B) 8 h; (C) 16 h; and (D) 24 h of transfection

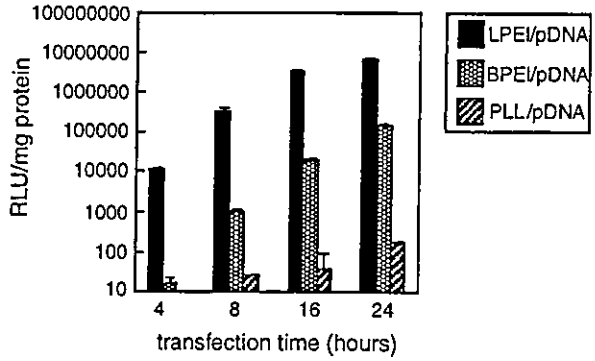

Figure 5. Time-dependent increase of luciferase gene expression with LPEI/pDNA, BPEI/pDNA, and PLL/pDNA polyplexes. After 4–24 h of transfection, the luciferase gene expression was measured using Fluoroscan Ascent FL (Dainippon, Japan). n = 6; ±SE

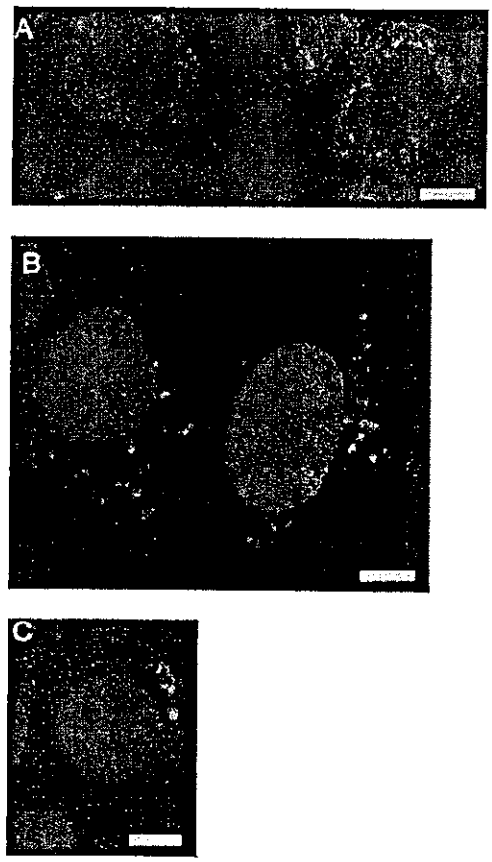

Figure 6. Fluorescent images after 24 h of transfection using fluorescein-labeled pDNA. The nucleus was stained with Hoechst 33258 prior to confocal microscopy for 15 min. Transfection with (A) LPEI/pDNA; (B) BPEI/pDNA; and (C) PLL/pDNA. Bar 10 μm

dissociation is considered to take place by an interexchange reaction of the complexed pDNA with the surrounding polyanion, such as cytoplasmic mRNA, phosphatidylserine, or anionic proteoglycan [23]. Thus, the feasibility of this interexchange reaction may distinctly affect gene expression and should be evaluated from the standpoint of its physicochemical properties.

By using the doubly labeled (fluorescein and X-rhodamine) pDNA, the interexchange reaction between the polyanion and the complexed pDNA in the LPEI, BPEI, and PLL/pDNA polyplexes was evaluated by FRET measurement [21]. Poly(aspartic acid) was used as the model counter-polyanion [24]. As shown in Figure 7, the LPEI and BPEI/pDNA polyplexes showed a rapid decrease in the emission intensity ratios, indicating that the DNA decondensation was induced by the dissociation from polycations. In contrast, the ratio of the PLL/pDNA polyplex decreased in a much slower manner. The tight binding of PLL with pDNA, resulting in the restricted release of pDNA through a chain exchange reaction, may have a role in the lower gene expression compared with PEI. Nevertheless, the kinetics of the decreased emission intensity ratios was not significant between LPEI and BPEI.

From a different viewpoint, it is worth noting that BPEI/pDNA had a remarkably higher initial intensity ratio than LPEI/pDNA. Since the intensity ratio is considered to reflect the condensation degree of pDNA, the BPEI/pDNA polyplexes are likely to induce a denser condensation of pDNA. This was further demonstrated by AFM (Figure 8). The polyplex diameters of LPEI and BPEI/pDNA were in a similar range, around 100 nm. These diameters were also confirmed by dynamic light scattering measurements (data not shown). However, in the cross section, the LPEI/pDNA polyplex was observed to have a multi-peak profile. In contrast, the BPEI/pDNA polyplex showed a taller and single-peak profile, suggesting a higher molecular density at the core of the complex. These results suggested that BPEI might induce the denser condensation of pDNA inside the polyplexes, which was in line with the higher FRET ratio of BPEI/pDNA.

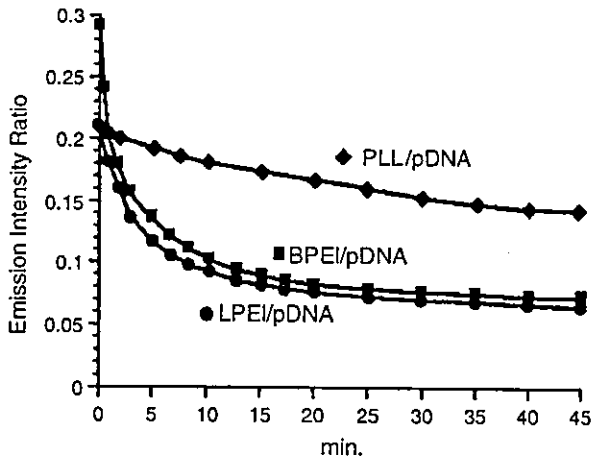

Figure 7. Interexchange reaction between poly(aspartic acid) and pDNA in the polyplexes. The LPEI, BPEI, and PLL/pDNA polyplexes were prepared by using the doubly labeled (fluorescein and X-rhodamine) pDNA. After measurement of the initial emission intensity ratio of X-rhodamine/fluorescein, poly(aspartic acid) solution was added, and, with gentle stirring, the time-dependent change of the emission intensity ratio was evaluated. (●) LPEI/pDNA; (■) BPEI/pDNA; and (♦) PLL/pDNA polyplexes

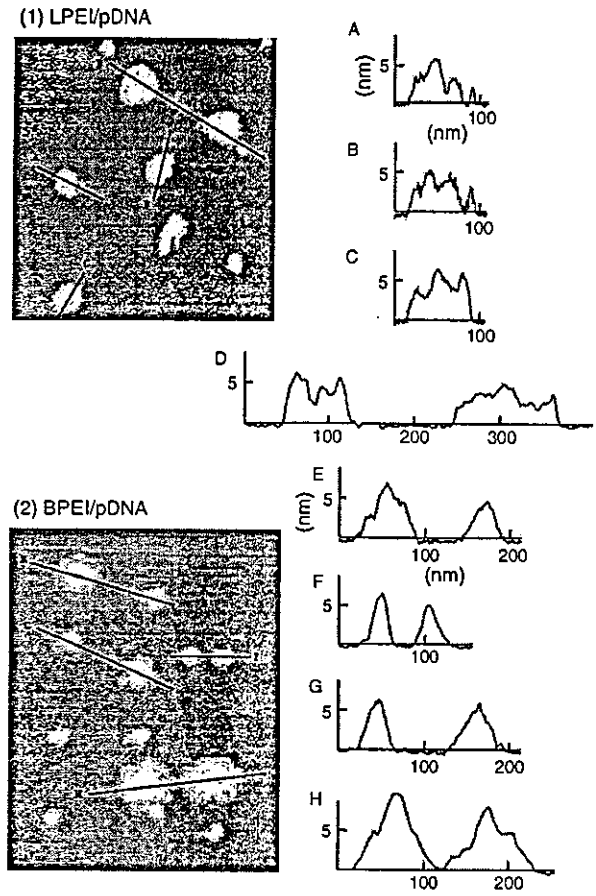

Figure 8. Atomic force microscopy of LPEI and BPEI/pDNA polyplexes. Each polyplex sample solution (5 μl) was deposited on a freshly cleaved mica substrate for 30 s. The solution was then rinsed with 50 μl of MilliQ deionized water (Millipore) and dried under a gentle nitrogen gas flow. AFM imaging was performed in the tapping mode with standard silicon probes (Olympus, Tokyo, Japan) on a NVB100 microscope (Olympus) controlled by Nanoscope IIIa software (Digital Instruments, USA). The cantilever oscillation frequency was tuned to the resonance frequency of the cantilever, 260–340 kHz. The 256 × 256 images were recorded at a 0.5–2 μm/s linear scanning speed at a sampling density of 4–60 nm^2 per pixel. The raw AFM images were processed only for background removal (flattening) using the software. (1) LPEI/pDNA and (2) BPEI/pDNA. The figures on the right are the cross sections at the lines indicated in the left-hand pictures (A–H)

Discussion

The process of transfection with non-viral gene delivery systems consists of many steps, such as the association of the DNA-loaded complexes with the cell surface, the internalization presumably by endocytosis, the escape from the endosomes, transport of the complexes or the released pDNA to the nucleus, and transcription in the nucleus. Each step may be a barrier to gene expression; however, the escape from the endosomes has been considered as one of the crucial obstacles. In this regard, PEI has been a promising candidate due to its buffering capacity under physiological pH conditions,

which is expected to induce endosomal rupture and enable polyplexes to escape without degradation. In fact, Akinc *et al.* reported that by using the fluorescent-labeled DNA, the pH environment of DNA inside the cells was measured as less acidic when delivered by BPEI and LPEI compared with PLL [25]. In contrast, it was also reported that an increase in pH was not observed around the PEI/pDNA polyplexes even by using a similar labeling method [26]. This inconsistency may be partly due to the difference in the labeling target, i.e., the former labeled the pDNA molecules and the latter the polymers. It is likely that the dissociation of the pDNA and polymers induces the discrepancy in their pH environments; however, details of their intracellular fate remain unclear.

These problems led us to this study focusing on the dissociation of pDNA from a cationic polymer. When released from the complexes, the pDNA should be decondensed from the condensed state inside the polyplexes. In the doubly labeled pDNA, the conformational change leads to a change in the distance between the two fluorescent molecules attached to a single pDNA molecule. Thus, pDNA decondensation through polyplex dissociation should be detected by FRET measurement [21]. Moreover, since this measurement can be carried out under physiological conditions, it is feasible to apply it for single cell observations under fluorescence microscopy.

In this study it was revealed that escape from the endosomes, presumably via the proton-sponge effect, was observed in the LPEI and BPEI/pDNA polyplexes. However, despite their identical chemical formulas, LPEI and BPEI showed a remarkable difference in intracellular behavior. LPEI presented a rapid and efficient pDNA decondensation in the cytoplasm, which was clearly correlated with the earlier detectable gene expression. In contrast, the BPEI/pDNA polyplexes were observed to remain in the condensed state even after 24 h of transfection.

Regardless of the condensation state of the pDNA, most of the fluorescent-labeled pDNAs was observed in the cytoplasm, suggesting that only a small portion of the internalized pDNA was transported to the nucleus. This is consistent with the restricted mobility of the high molecular DNA in the cytoplasm as reported by Lukacs *et al.* [27]. Note that even a single molecule of DNA with an applicable conformation for the transcription can repeatedly produce the mRNA, playing a key role, in a time-dependent manner, in determining the amount of the synthesized protein. It is thus suggested that the rapid and excellent gene expression is correlated with the increase in the concentration of intra-cytoplasmic pDNA undergoing smooth decondensation.

The BPEI/pDNA polyplexes were observed to remain mostly complexed in the cytoplasm. A similar result was reported by Godbey *et al.* [28]. They showed that by microscopic observation of the intracellular trafficking of the BPEI/pDNA polyplexes using separately labeled DNA and BPEI, both pDNA and BPEI were observed co-localizing in the nucleus as well as in the cytoplasm. These observations suggested that a portion of the BPEI/pDNA polyplexes was transported to the nucleus; however, the polymer and pDNA still remained complexed. Such a complexed pDNA is obviously unfavorable for transcription. This excessive stabilization of BPEI/pDNA polyplexes may cause lower gene expression compared with LPEI.

From the standpoint of physicochemical properties, the interexchange kinetics of pDNA and poly(aspartic acid) did not reveal any difference between LPEI and BPEI. However, the FRET analysis and the observations by AFM indicated that their structures were obviously different. Compared with LPEI, the BPEI/pDNA polyplex showed the more condensed structure. Consequently, in the cytoplasm, pDNA dissociation from BPEI is likely to be more difficult and a more time-requiring process than from LPEI.

On the other hand, PLL made a striking contrast both in intracellular behavior as well as the interexchange reaction. After transfection, the PLL/pDNA polyplexes were mostly entrapped in the endosomes, presumably due to the lack of the proton-sponge effect. In addition, the feasibility of the pDNA dissociation from PLL was found to be much less than that of PEI, indicating that the PLL/pDNA polyplexes are, in a sense, too stable in the cells. These PLL properties are thought to cause the significantly lower transfection efficiency compared with PEI. However, we recently observed that, even by using the PLL-based polymer systems, the sufficiently long incubation in the presence of chloroquine could produce a significant enhancement in gene expression (unpublished data), suggesting that dissociation of pDNA from PLL may be accomplished by the longer incubation.

In conclusion, the superiority of LPEI as a polyplex component is considered to be the rapidity of gene expression due to the smooth intracellular disintegration of the complex with pDNA. This property may be particularly beneficial to achieve an appreciably high gene expression in a prompt manner.

Acknowledgements

This work was financially supported by Grants-in-Aid for Scientific Research (no. 11167210 to K.K and no. 12877221 to H.K.) and Special Coordination Funds for Promoting Science and Technology from the Ministry of Education, Culture, Sports, Science and Technology of Japan as well as by the Core Research Program for Evolutional Science and Technology (CREST) from the Japan Science and Technology Corporation (JST).

References

1. Han S, Mahato RI, Sung YK, Kim SW. Development of biomaterials for gene therapy. *Mol Ther* 2000; 2: 302–317.
2. Kabanov AV. Taking polycation gene delivery systems from in vitro to in vivo. *Pharm Sci Technol Today* 1999; 2: 365–372.
3. De Smedt SC, Demeester J, Hennink WE. Cationic polymer based gene delivery systems. *Pharm Res* 2000; 17: 113–126.
4. Boussif O, Lezoualc'h F, Zanta MA, *et al.* A versatile vector for gene and oligonucleotide transfer into cells in culture and

in vivo: polyethylenimine. *Proc Natl Acad Sci U S A* 1995; 92: 7297–7301.
5. Boussif O, Zanta MA, Behr JP. Optimized galenics improve in vitro gene transfer with cationic molecules up to 1000-fold. *Gene Ther* 1996; 3: 1074–1080.
6. Behr JP. The proton sponge: a trick to enter cells the viruses did not exploit. *Chimia* 1997; 51: 34–36.
7. Abdallah B, Hassan A, Benoist C, Goula D, Behr JP, Demeneix BA. A powerful nonviral vector for in vivo gene transfer into the adult mammalian brain: polyethylenimine. *Hum Gene Ther* 1996; 7: 1947–1954.
8. Kircheis R, Kichler A, Wallner G, *et al.* Coupling of cell-binding ligands to polyethylenimine for targeted gene delivery. *Gene Ther* 1997; 4: 409–418.
9. Ogris M, Steinlein P, Kursa M, Mechtler K, Kircheis R, Wagner E. The size of DNA/transferrin-PEI complexes is an important factor for gene expression in cultured cells. *Gene Ther* 1998; 5: 1425–1433.
10. Fischer D, Bieber T, Li Y, Elsasser HP, Kissel T. A novel nonviral vector for DNA delivery based on low molecular weight, branched polyethylenimine: effect of molecular weight on transfection efficiency and cytotoxicity. *Pharm Res* 1999; 16: 1273–1279.
11. Ferrari S, Moro E, Pettenazzo A, Behr JP, Zacchello F, Scarpa M. ExGen 500 is an efficient vector for gene delivery to lung epithelial cells in vitro and in vivo. *Gene Ther* 1997; 4: 1100–1106.
12. Goula D, Remy JS, Erbacher P, *et al.* Size, diffusibility and transfection performance of linear PEI/DNA complexes in the mouse central nervous system. *Gene Ther* 1998; 5: 712–717.
13. Bragonzi A, Boletta A, Biffi A, *et al.* Comparison between cationic polymers and lipids in mediating systemic gene delivery to the lungs. *Gene Ther* 1999; 6: 1995–2004.
14. Li S, Tan Y, Viroonchatapan E, Pitt BR, Huang L. Targeted gene delivery to pulmonary endothelium by anti-PECAM antibody. *Am J Physiol Lung Cell Mol Physiol* 2000; 278: L504–L511.
15. Poulain L, Ziller C, Muller CD, *et al.* Ovarian carcinoma cells are effectively transfected by polyethylenimine (PEI) derivatives. *Cancer Gene Ther* 2000; 7: 644–652.
16. Wightman L, Kircheis R, Rossler V, *et al.* Different behavior of branched and linear polyethylenimine for gene delivery in vitro and in vivo. *J Gene Med* 2001; 3: 362–372.
17. Brunner S, Furtbauer E, Sauer T, Kursa M, Wagner E. Overcoming the nuclear barrier: cell cycle independent nonviral gene transfer with linear polyethylenimine or electroporation. *Mol Ther* 2002; 5: 80–86.
18. Suh J, Paik H-J, Hwang BK. Ionization of poly(ethylenimine) and poly(allyamine) at various pH's. *Bioorg Chem* 1994; 22: 318–327.
19. Godbey WT, Wu KK, Mikos AG. Size matters: molecular weight affects the efficiency of poly(ethylenimine) as a gene delivery vehicle. *J Biomed Mater Res* 1999; 45: 268–275.
20. Gebhart CL, Kabanov AV. Evaluation of polyplexes as gene transfer agents. *J Control Release* 2001; 73: 401–416.
21. Itaka K, Harada A, Nakamura K, Kawaguchi H, Kataoka K. Evaluation by fluorescence resonance energy transfer of the stability of nonviral gene delivery vectors under physiological conditions. *Biomacromolecules* 2002; 3: 841–845.
22. Kichler A, Leborgne C, Coeytaux E, Danos O. Polyethylenimine-mediated gene delivery: a mechanistic study. *J Gene Med* 2001; 3: 135–144.
23. Labat-Moleur F, Steffan AM, Brisson C, *et al.* An electron microscopy study into the mechanism of gene transfer with lipopolyamines. *Gene Ther* 1996; 3: 1010–1017.
24. Katayose S, Kataoka K. Water-soluble polyion complex associates of DNA and poly(ethylene glycol)-poly(L-lysine) block copolymer. *Bioconjug Chem* 1997; 8: 702–707.
25. Akinc A, Langer R. Measuring the pH environment of DNA delivered using nonviral vectors: implications for lysosomal trafficking. *Biotechnol Bioeng* 2002; 78: 503–508.
26. Forrest ML, Pack DW. On the kinetics of polyplex endocytic trafficking: implications for gene delivery vector design. *Mol Ther* 2002; 6: 57–66.
27. Lukacs GL, Haggie P, Seksek O, Lechardeur D, Freedman N, Verkman AS. Size-dependent DNA mobility in cytoplasm and nucleus. *J Biol Chem* 2000; 275: 1625–1629.
28. Godbey WT, Wu KK, Mikos AG. Tracking the intracellular path of poly(ethylenimine)/DNA complexes for gene delivery. *Proc Natl Acad Sci U S A* 1999; 96: 5177–5181.

Available online at www.sciencedirect.com
SCIENCE DIRECT®
Biochemical and Biophysical Research Communications 313 (2004) 503–508
BBRC
www.elsevier.com/locate/ybbrc

A new technique to expand human mesenchymal stem cells using basement membrane extracellular matrix

Takehiro Matsubara,[a,c,f] Shinichi Tsutsumi,[b] Haiou Pan,[a] Hisatada Hiraoka,[c] Ryo Oda,[d] Masahiro Nishimura,[e] Hiroshi Kawaguchi,[c] Kouzou Nakamura,[c] and Yukio Kato[a,f,*]

[a] *Japan Science and Technology Corporation (JST), Chiyoda-ku, Tokyo 102-8666, Japan*
[b] *Department of Orthopedic Surgery, School of Medicine, Gunma University, Maebashi 371-8511, Japan*
[c] *Department of Orthopedic Surgery, Graduate School of Medicine, University of Tokyo, Tokyo 113-8655, Japan*
[d] *Department of Operative Dentistry, Graduate School of Biomedical Science, Hiroshima University, Hiroshima 734-8553, Japan*
[e] *Department of Prosthetic Dentistry, Graduate School of Biomedical Science, Hiroshima University, Hiroshima 734-8553, Japan*
[f] *Department of Dental and Medical Biochemistry, Graduate School of Biomedical Science, Hiroshima University, Hiroshima 734-8553, Japan*

Received 12 November 2003

Abstract

Mesenchymal stem cells (MSC) show a very short proliferative life span and readily lose the differentiation potential in culture. However, the growth rate and the proliferative life span of the stem cells markedly increased using tissue culture dishes coated with a basement membrane-like extracellular matrix, which was produced by PYS-2 cells or primary endothelial cells. Furthermore, the stem cells expanded on the extracellular matrix, but not those on plastic tissue culture dishes, retained the osteogenic, chondrogenic, and adipogenic potential throughout many mitotic divisions. The extracellular matrix had greater effects on the proliferation of MSC and the maintenance of the multi-lineage differentiation potential than basic fibroblast growth factor. Mesenchymal stem cells expanded on the extracellular matrix should be useful for regeneration of large tissue defects and repeated cell therapies, which require a large number of stem or progenitor cells.

Keywords: Mesenchymal stem cell; Basement membrane; Extracellular matrix; Regeneration; Differentiation

Mesenchymal stem cells (MSC) can be induced to differentiate into a variety of tissues including bone, cartilage, tendon, fat, heart, muscle, and brain, in vitro and in vivo [1,2]. Autologous MSC have advantages over ES cells: there is no teratocarcinoma formation, no immune rejection, and there are no ethical problems. However, compared with ES cells, which have an unlimited proliferative life span (period before the cells reach growth arrest in culture) and consistently high telomerase activity, MSC have very poor replicative capacity and short proliferative longevity [3,4]. Thus, an important challenge in regenerative medicine is to improve the replicative capacity of MSC, thereby to obtain a number of MSC sufficient to repair large defects. Forced expression of telomerase in MSC markedly increases their proliferative life span and MSC with a high telomerase activity showed osteogenic potential [5]. However, it is unknown whether these cells can maintain the chondrogenic and adipogenic potential or whether these cells have a risk of transformation. We report here that the growth rate and the proliferative life span of MSC markedly increased using tissue culture dishes coated with a basement membrane-like extracellular matrix ("bmECM"). Furthermore, MSC that expanded 10^6-fold on bmECM retained its osteogenic, chondrogenic, and adipogenic potential.

Materials and methods

Preparation of bmECM-coated dishes. PYS-2 cells, which produce laminin, type IV collagen, and heparan sulfate proteoglycans [6–8], were supplied by Dr. Atsumi (Riken, Wako, Japan), and bovine corneal endothelial cells were isolated and maintained as described [9].

* Corresponding author. Fax: +81-82-257-5629.
E-mail address: ykato@hiroshima-u.ac.jp (Y. Kato).

0006-291X/$ - see front matter © 2003 Elsevier Inc. All rights reserved.
doi:10.1016/j.bbrc.2003.11.143

BmECM-coated dishes were prepared according to the method of Dr. Gospodarowicz [10]. The cells were seeded at 2×10^4 cells/cm^2 on 60-mm tissue culture dishes (Corning, Corning, NY) and maintained in 4 ml of Dulbecco's modified Eagle's medium (DMEM)-Ham's F12 medium (1:1) (Sigma, St. Louis, MO) in the presence of 10% fetal bovine serum (Hyclone, Logan, Utah) and antibiotics (100 U/ml penicillin G and 100 μg/ml streptomycin) (medium-A). Medium was changed every other day. Once the cultures became confluent, the media were renewed by 4 ml of medium-A supplemented with 5% dextran (200,000 Da, Wako, Osaka, Japan) and the cultures were further incubated for 7 days. Treatment of the cultures with 20 mM NH_3 resulted in cell lysis, exposing the extracellular matrix adhering to the substrata of tissue culture dishes. The substratum was washed five times with PBS. Previous studies have shown that bmECM is composed of laminin, heparan sulfate, entactin, and type IV collagen [11,12].

Preparation of laminin-coated dishes, type IV collagen-coated dishes, and ECM gel-coated dishes. Three milliliters of 10 mM $NaHCO_3$ containing 30 μg/ml type IV collagen or 30 μg/ml laminin (Koken, Tokyo, Japan) was incubated in 60-mm plastic tissue culture dishes at 4 °C for 12 h. Two hundred micrograms per milliliter ECM gel solution (Sigma) was made by diluting with DMEM-high glucose. Three milliliters of the ECM gel solution was incubated in 60-mm tissue culture dishes at 4 °C for 12 h. These concentrations of laminin, type IV collagen, and ECM gel were optimal for proliferation of MSC (data not shown).

MSC culture. Human MSC were obtained from the ilium or the alveolar bone according to a protocol approved by ethical authorities at Hiroshima University. Cells in marrow aspirates (1 ml/100-mm dish) were seeded on plastic tissue culture dishes. Passages were performed when cells were approaching confluence. Unless otherwise specified, MSC obtained from the primary cultures were seeded at 1×10^3 cells/cm^2 on 60-mm of laminin-, type IV collagen- or ECM gel-coated dishes, on bmECM-coated dishes or on plastic tissue culture dishes, and cells were fed with DMEM-low glucose supplemented with 10% fetal bovine serum and antibiotics (medium-B) every 3 days. Subsequent passages were performed on the appropriate substrata. In these studies, we seeded MSC at a low density (1×10^3 cells/cm^2) to avoid frequent passages and the risk of contamination considering clinical application, although MSC showed a higher growth rate and a longer proliferative life span at a high seeding cell density (5×10^3 cells/cm^2) (data not shown).

Differentiation. Chondrogenic, osteogenic or adipogenic conversion of MSC was determined according to the procedures reported by Pittenger et al. [1], with some modifications. For chondrogenic differentiation, cells were seeded at 2.5×10^5 cells per 15 ml plastic centrifuge tube and maintained in 0.5 ml of serum-free α-MEM supplemented with 3500 mg/ml glucose, 6.25 μg/ml insulin, 6.25 μg/ml transferrin, 6.25 ng/ml selenite, 5.33 μg/ml linolate, 1.25 mg/ml bovine serum albumin, 10 ng/ml transforming growth factor-β3, 100 nM dexamethasone, and 50 μg/ml ascorbic acid-2-phosphate. The cultures were fed with 0.5 ml of the medium until 3 days after seeding. Thereafter, the cultures were fed with 1 ml of the medium every other day. Cells were cultured under the chondrogenic status for 28 days. For osteogenic differentiation, cells were seeded at 4×10^4 cells per 16-mm dish and maintained for 21–28 days in DMEM-low glucose supplemented with 10 μg/ml insulin, 10 mM β-glycerophosphate, 100 nM dexamethasone, and 50 μg/ml ascorbic acid-2-phosphate. For adipogenic differentiation, cells were seeded at 2×10^5 cells per 35-mm dish and grown to confluence in medium-B. Thereafter, adipogenic differentiation was induced by subjecting confluent monolayers to 3–4 rounds of adipogenic treatments. Each round had two steps; incubation with adipogenic medium (DMEM-high glucose, 10% fetal bovine serum, 0.2 mM indomethacin, 1 μM dexamethasone, 0.5 mM methyl-isobutylxanthine, and 10 μg/ml insulin) for 72–96 h and incubation with maintenance medium (DMEM-high glucose, 10% fetal bovine serum, and 10 μg/ml insulin) for 72–96 h. Cells were cultured under the adipogenic status for 28 days.

Glycosaminoglycan content, alkaline phosphatase activity, calcium level, glycerol-3-phosphate dehydrogenase activity, and DNA content. The glycosaminoglycan (GAG) content was determined using a sulfated GAG assay kit (Biocolor, Newtownabbey, UK) [13]. The alkaline phosphatase (ALP) activity was determined by the method of Bessey [14]. The calcium level was determined by the method of Gitelman [15]. The glycerol-3-phosphate dehydrogenase activity was determined using an assay kit (Hokudo, Sapporo, Japan) [16]. The DNA content was determined using a fluorescent DNA quantification kit (Bio-Rad, Chicago, IL).

RT-PCR. Total RNA was extracted using Isogen (Nippon Gene, Tokyo, Japan). The first-strand cDNA was synthesized from 1 μg of total RNA using the SUPERSCRIPT II RNase H$^-$ reverse transcriptase (Life Technologies, Rockville, MD). Using the cDNAs as a template, PCR was carried out under the following conditions: denaturation at 94 °C for 30 s and primer extension at 65 °C for 1.5 min in 27 cycles. Pairs of nucleotides, 5′-TGGTGGAGCAGCAAGAGCAA-3′ and 5′-TGCCCAGTTCAGGTCTCTTA-3′ for type II collagen, 5′-CCCAACACCAAGACACAGTT-3′ and 5′C-ATCACCTTTGATG CCTGGCT-3′ for type X collagen, and 5′-GTCAAGGCCGAGAAT GGGAA-3′ and 5′-GCTTCACCACCTTCTTGATG-3′ for GAPDH, 5′-CATTTTGGGAATGGCCTGTG-3′ and 5′-ATTGTCTCCTCCG CTGCTGC-3′ for bone sialoprotein, 5′-CTAGGCATCACCTGTGC CATACC-3′ and 5′-CAGTG ACCAGTTCATCAGATTCATC-3′ for osteopontin, 5′-CCACCGAGACACCATGAGAG-3′ and 5′-CCATA GGGCTGGGAGGTCAG-3′ for osteocalcin, and 5′-CATTCTGGC CCACCAACTT-3′ and 5′-CCTTGCA TCCTTCACAAGCA-3′ for PPAR-γ2 were used as primers for RT-PCR. Obtained PCR products were separated on 1% agarose gels and stained with ethidium bromide.

Statistical analysis. Student's *t* test was used.

Results

The extracellular matrix produced by PYS-2 cells or endothelial cells adhered to the substratum of plastic tissue culture dishes and could be easily cut with a needle and turned over like a sheet of paper (Fig. 1A). When cells in marrow aspirates were seeded on plastic culture dishes, adherent cells—MSC—proliferated in the presence of 10% fetal bovine serum at a high growth rate in primary cultures [3], but their growth rate rapidly decreased in secondary and tertiary cultures (Figs. 1B–D). In cultures on plastic tissue culture dishes, non-adherent cells were removed completely by the first passage. However, when cells in marrow aspirates were seeded directly on bmECM, both MSC and many other cells adhered to the substratum and these adherent cells were not removed by changing the medium. Accordingly, we harvested MSC when the cells were approaching confluence in primary cultures on plastic tissue culture dishes, and seeded the isolated MSC on bmECM or plastic tissue culture dishes without the matrix ("plastic") to examine the effects of bmECM on the proliferation of MSC.

The growth rate of human MSC isolated from the ilium (Fig. 1B) or the alveolar bone (Fig. 1C) on bmECM was much higher than that on plastic, and thus the cumulative cell number in the cultures on bmECM was 10^5-fold greater than that on plastic on day 50. After MSC obtained from primary cultures were seeded

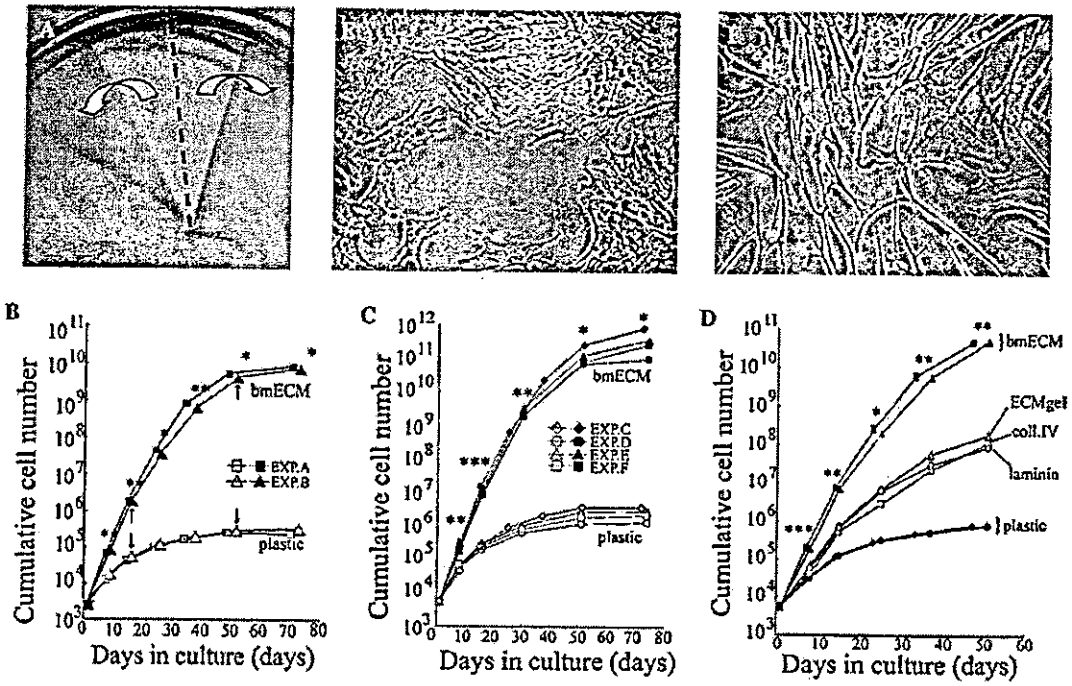

Fig. 1. Expansion of human MSC on ECM-coated dishes. (A) The gross appearance of bmECM. (B) Cells in marrow aspirates (1 ml/100-mm dish) from the ilium of two volunteers (EXP. A in her 50s and EXP. B in her 80s) were seeded on plastic tissue culture dishes. MSC were harvested when the cells were approaching confluence in primary cultures, and the isolated cells were seeded on bmECM produced by PYS-2 cells or on plastic (the first passage cultures), as described in Materials and methods. Subsequently, passages were performed on the appropriate substrata. *,**Differs significantly from the cell number in cultures on plastic dish on days 7–8, 14–15, 23–25, 33–37, 47–51 or 68–72 ($*p < 0.05$, $**p < 0.01$). Arrows: MSC obtained from the 2nd passage culture on day 15 or MSC from the 5th passage culture on day 51 were transferred into chondrogenic, osteogenic, and adipogenic status. (C) MSC obtained from the alveolar bone of four volunteers (EXP. C,D in their 20s and EXP. E,F in their 80s) were cultured on plastic or bmECM produced by bovine corneal endothelial cells, as described above. *,**,***Differs significantly from the cell number in cultures on plastic dish on day(s) 7–8, 14–15, 30, 51, 47–51 or 72–74 ($*p < 0.05$, $**p < 0.01$, and $***p < 0.001$). (D) MSC obtained from the ilium were cultured on laminin-, type IV collagen-, ECM gel-coated dishes, bmECM or plastic, as described above. *,**,***Differs significantly from the cell number in cultures on laminin-, type IV collagen- or ECM gel-coated dishes on days 7–8, 14–15, 23–25, 33–37 or 47–51 ($*p < 0.05$, $**p < 0.01$, and $***p < 0.001$). (E,F) Flat and spindle-like cell shape on plastic (E) and bmECM (F), (40×) (on day 45 in the 5th passage cultures).

on bmECM or plastic, the proliferative life span of MSC on bmECM (50.3 ± 1.5 days) was also significantly ($p < 0.0001$) longer than that of MSC on plastic (29.2 ± 4.4 days) (Figs. 1B and C). The effect of bmECM produced by PYS-2 was similar to that of endothelial cell bmECM (Fig. 1). MSC seeded at a low density and grown on plastic lost their spindle-like appearance, becoming flat with an increase in the passage number (Fig. 1E). The flat appearance is characteristic of senescent cells. However, most MSC grown on bmECM maintained the spindle-like appearance until the 5th passage culture on day 45 (Fig. 1F), suggesting that bmECM suppressed cell senescence.

Laminin and type IV collagen are the major components of bmECM, but MSC on laminin- or type IV collagen-coated dishes showed lower growth rates than on bmECM (Fig. 1F). The ECM gel isolated from Engelbreth–Holm–Swarm murine sarcoma also showed less growth stimulation than bmECM (Fig. 1F), suggesting a loss of active substances during isolation of the extracellular matrix components or the necessity of an intact structure for growth stimulation.

The chondrogenic potential of MSC was examined as a function of the passage number. MSC obtained from the 2nd and the 5th passage cultures on day 15 and day 51 (Fig. 1B) were maintained in pellet cultures for 28 days (Fig. 2A). The amount of cartilage proteoglycan stained with toluidine blue was greater in the pellets obtained from the 5th passage cultures grown on bmECM than in the pellets from the 2nd and the 5th passage cultures grown on plastic. The expressions of type II collagen and type X collagen mRNAs were higher in pellets from the 5th passage cultures on bmECM than in pellets from the 5th passage cultures on plastic (Fig. 2B). GAG content and ALP activity in the pellets decreased with the increase in the passage number, irrespective of the presence or absence of bmECM. However, at each passage number, the GAG content (Fig. 2C) and ALP activity (Fig. 2D) were higher with MSC from cultures on bmECM than with MSC from cultures on plastic.

Next, MSC from the 2nd and the 5th passage cultures on bmECM or plastic were incubated under the osteogenic status on plastic tissue culture dishes. During

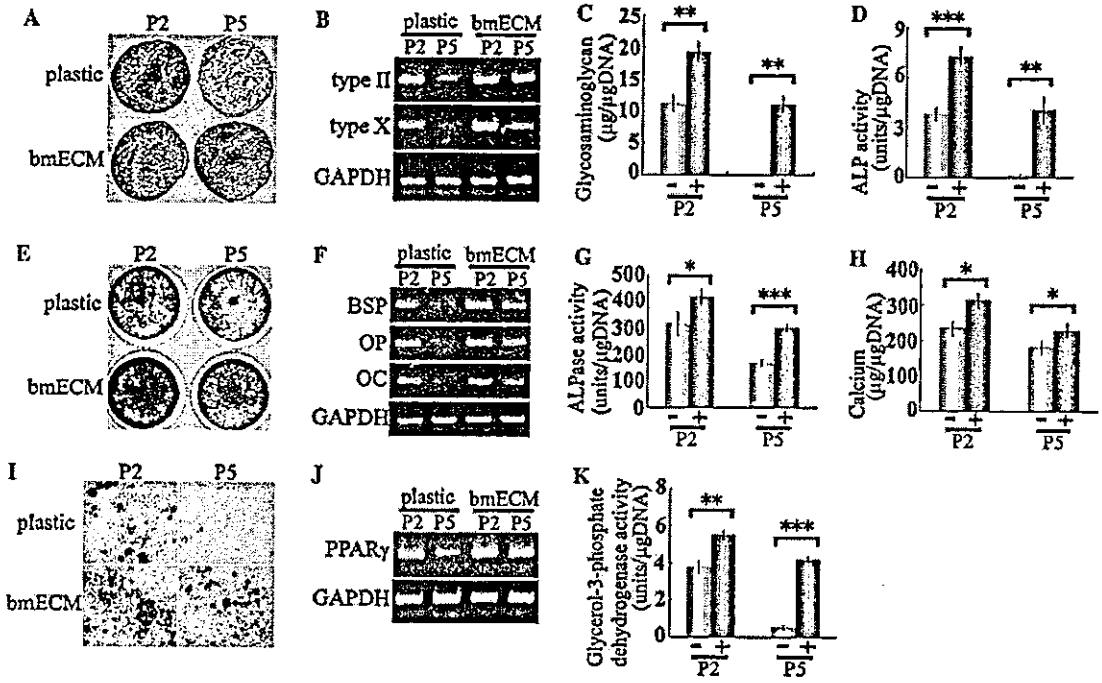

Fig. 2. Retention of chondrogenic, osteogenic, and adipogenic potential on bmECM. The MSC obtained from the 2nd and the 5th passage cultures on plastic or bmECM produced by PYS-2 cells (Fig. 1B) were transferred into the chondrogenic status in pellet cultures for 28 days (A–D) and stained with toluidine blue (A). (B) The mRNA levels of type II collagen (type II) and type X collagen (type X) were analyzed by RT-PCR. GAG content (C) and ALP activity (D) were determined on day 28. The MSC from the 2nd and the 5th passage cultures on plastic or bmECM were transferred into the osteogenic status (E–H). (E) The cell layers were stained with alizarin red on day 21. (F) The mRNA levels of bone sialoprotein (BSP), osteopontin (OP), and osteocalcin (OC) were analyzed by RT-PCR on day 28. The ALP activity (G) and calcium level (H) of the cell-matrix layers were determined on day 28. The MSC obtained from the 2nd and the 5th passage cultures on plastic or bmECM were cultured under the adipogenic status for 28 days (I–K). (I) The cell layers were stained with oil-red O. (J) The mRNA level of PPAR-γ2 was analyzed by RT-PCR. (K) Glycerol-3-phosphate dehydrogenase activity was determined. (C,D,G,H, and K) "−" and "+" represent MSC from culture on plastic and bmECM, respectively. Values are averages +/− SD for four cultures. $*p < 0.05$, $**p < 0.01$, and $***p < 0.001$ vs plastic.

osteogenesis, we did not use bmECM to discriminate the effect of the extracellular matrix on proliferation from its direct effect on differentiation. MSC from cultures on bmECM became stained with alizarin red more intensely than MSC from cultures on plastic on day 21 (Fig. 2E). The expressions of bone sialoprotein, osteopontin, and osteocalcin mRNAs on day 28 were also higher in cultures of MSC from cultures on bmECM than in cultures of MSC from cultures on plastic at the 5th passage (Fig. 2F). ALP activity and calcium level on day 28 decreased with the increase in the passage number. However, MSC from cultures on bmECM showed a higher ALP activity (Fig. 2G) and a higher calcium level (Fig. 2H) than MSC from cultures on plastic at the 2nd and the 5th passages.

To examine the adipogenic potential, MSC from the 2nd and the 5th passage cultures on bmECM or plastic were incubated under the adipogenic status on plastic tissue culture dishes for 28 days. MSC from cultures on bmECM showed higher adipogenic differentiation, which was indicated by more intense staining with oil-red O (Fig. 2I), higher PPAR-γ2 mRNA expression (Fig. 2J), and higher glycerol-3-phosphate dehydrogenase activity (Fig. 2K).

Next, human MSC were grown on bmECM or plastic with 10% human serum, since human serum may be safer than fetal bovine serum for clinical use. Under these conditions, MSC proliferated more rapidly and showed a longer proliferative life span on bmECM than on plastic (Fig. 3A). Furthermore, this effect of bmECM was greater than that of basic fibroblast growth factor (FGF). The MSC grown on bmECM for 66 days developed into a cartilage-like tissue (Fig. 3B), even though these MSC on bmECM had lost proliferation capability. In contrast, scarcely any cartilage-like tissue was formed with MSC obtained from 66-day-old cultures on plastic (Fig. 3C).

Discussion

The extracellular matrix (ECM) plays a vital role in organ morphogenesis, maintenance, and reconstruction following injury, and actions of ECM can be attributed to its effect on proliferation of stem cells, since stem cells reside on the basement membrane in the epithelium and some other tissues [17]. In muscle, satellite cells (stem cells)—which can be induced to differentiate into muscle,